Chapter 3: Discovery of PAS selective acetylcholinesterase inhibitors

3.1 Introduction

Acetylcholinesterase (AChE), a 3.5 kDa protein, is a member of carboxylesterase family with α/β-hydrolase fold [1]. The leading role of AChE is hydrolysis of synaptic acetylcholine (ACh) and regulation of cholinergic neurotransmission in the body. It also plays a pivotal role in neuritogenesis, synaptogenesis, amyloidosis, dopamine neuron activation, regulation of apoptosis, nerve regeneration, hematopoiesis, and lymphocyte activation [2, 3]. The *in vitro* and *in vivo* exercises explain the relationship between amyloid precursor protein (APP) processing and cholinergic activation through muscarinic and nicotinic receptors [4, 5].

Structurally, AChE consists of 'large central mixed β-sheets' surrounded by '15 α-helices' [6]. The anionic catalytic site (CAS) is located at the bottom of a narrow gorge of AChE consisting of esteratic site (Ser203, Glu334, and His447) and anionic site (Trp86). Another site, named as peripheral anionic site (PAS) consisting of Tyr72, Asp74, Tyr124, Trp286, and Tyr341 residues, is 20 Å from the catalytic center. The aromatic residue's ring creates 40% surface of gorge and is located in the loop, thus presenting greater conformational flexibility. Trp86 residue forms π-cation interaction with quaternary nitrogen of ACh along with Phe338 [7]. PAS of AChE acts as an adhesion site to non-amyloidogenic conformer of Aβ, leading to its conformational change to produce amyloid fibrils [8]. Trp286 at the PAS site mimics response of the whole enzyme on amyloid formation [9]. Further, AChE-Aβ complexes induce neurotoxicity and trigger more neurodegeneration than Aβ peptide alone. Thus,

designing AChE inhibitor (AChEI), that blocks PAS of the enzyme, will prevent Aβ aggregation as well as enhance cholinergic transmission for treating AD.

Both, β-amyloid protein (Aβ) and abnormally hyperphosphorylated tau (P-tau) can influence AChE overexpression in AD [10]. The improvement of cholinergic transmission by using AChEI may boost cognitive impairment of patients with schizophrenia [11, 12], and Parkinson's disease (PD) [13]. The Acetylcholine receptors, at neuromuscular junction, are reduced in myasthenia gravis (MG) [14], and AChEIs are considered essential for the treatment of MG. AChEIs can enhance cholinergic up-regulation by weakening the effect of neuroinflammation via immunocompetent cells expressing α-7-acetylcholine receptor (AChR) [15].

Butyrylcholinesterase (BuChE) level is increased by up to 2-fold during mild to moderate AD [16], and causes an imbalance between synthesis or synaptic release of ACh and its enzymatic hydrolysis. Therefore, AChEI with BuChE inhibition properties may provide better therapeutic result in neurological disorders.

The drug discovery process is time-consuming and cumbersome, but the use of *in-silico* approaches helps to identify better hits and scaffolds for a target. The pharmacophore modeling is a mathematical modeling technique, which may help in quick prediction of hits. The combination of ligand-based and structure-based pharmacophore models help in better productivity of outcome [17]. Earlier, researchers attempted to develop pharmacophore models and utilized them for virtual screening of database molecules to find new AChE inhibitors [18-23].

Present study combines both ligand-based (3D-QSAR) and energy optimized structure-based pharmacophore (e-pharmacophore) approaches for virtual screening of free ‘ZINC15’ database molecules. The hits, as AChE inhibitors, were recognized by utilizing HTVS and molecular docking studies of pharmacophore matched compounds

after removal of pan-assay interference compounds (PAINS) [24]. The workflow of hit identification based on ligand-based 3D-QSAR and structure-based e-pharmacophore is explicit in **Figure 3.1**.

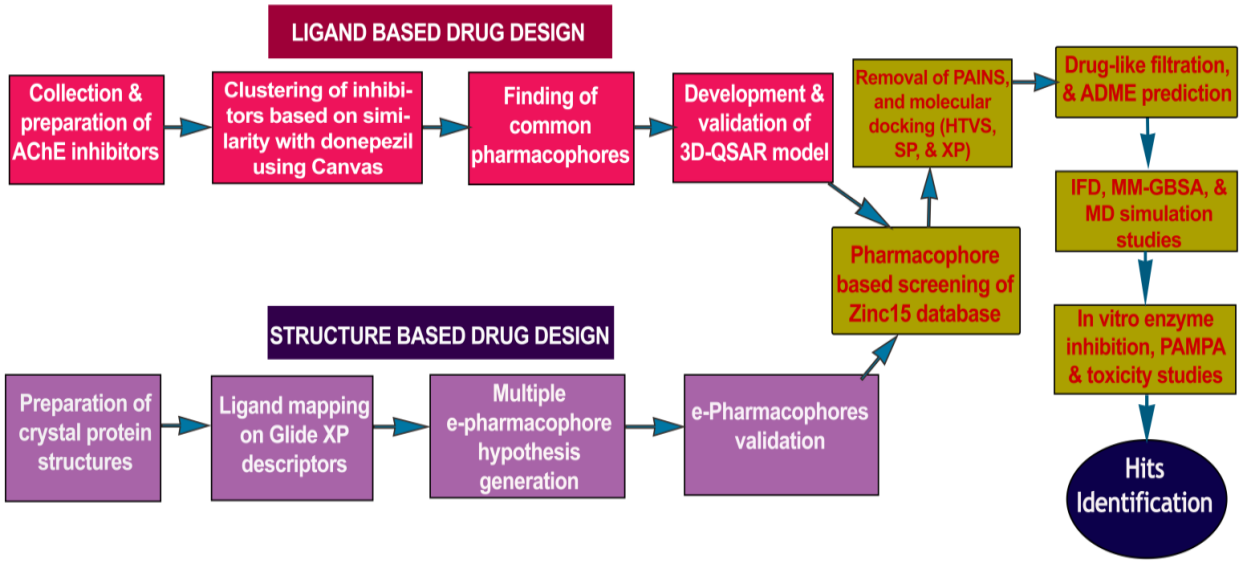

Figure 3.1 Flowchart of hit(s) identification based on ligand-based and structure-based pharmacophore models.

The *in vitro* studies, *i.e.*, enzyme inhibitions (AChE & BuChE), enzyme kinetics (AChE), propidium iodide displacement from AChE, parallel artificial membrane permeability assay for blood-brain barrier (PAMPA-BBB), effects on cell viability and neuroprotectivity against apoptosis triggered by L-glutamate, approved and validated the outcome of *in-silico* study.

3.2 Materials and Methods

3.2.1 Computational details

The computational details to develop structure-based and ligand-based pharmacophore models for the screening of publicly free 'ZINC15' database and MD simulations have been discussed in Chapter 2, Section 2.2.1.

3.2.2 Development of ligand-based pharmacophore

Total 1062 structurally diverse AChE inhibitors with known and wide range of IC_{50} values (0.043−20000 nM) were collected from Binding DB database (2017). The LigPrep in Maestro was utilized to minimize the energy of inhibitor molecules by applying OPLS_2005 force field [25]. As donepezil has mixed type (PAS and CAS site) of binding properties with AChE, therefore, all the compounds were clustered by Tanimoto similarities against donepezil using linear fingerprint descriptors with Canvas v2.3. Compounds were collected depending upon canvas similarity higher than and equal to 0.15 and molecular weight below 500. Finally, 142 inhibitors (Appendix, **Figure A.2**) were selected based on Glide docking study at PAS of AChE. The IC_{50} values of inhibitors were converted to pIC_{50} for the generation of 3D-QSAR model. PHASE v4.2 was used to generate 3D-QSAR model [26]. The ConfGen was used to create maximum 1000 number of conformers per structure utilizing force field OPLS_2005. The threshold of actives was above 8.0 and inactives was below 5.7. The PHASE randomly divided all ligands into two sets, *i.e.*, test set of 42, and training set of 100 compounds, to develop an Atom-based 3D-QSAR model in 1.00 Å of grid spacing. The ligands used for development of pharmacophore hypothesis are listed (Appendix, **Table A.2**) with their fitness score, observed pIC_{50}, PHASE predictive activity, and errors (the difference between observed and predicted activity). The common pharmacophore was obtained from the score of hypotheses having best alignment of the active set ligands. All 142 compounds were aligned with the template pharmacophore hypothesis of highly active molecule (**Figure 3.2**).

3.2.3 Validation of ligand-based pharmacophore

QSAR model was developed with partial least-squares (PLS) factors one to five and was validated by predicting pIC_{50} value of molecules. The QSAR model with PLS

factor 5 was considered as best model. 3D-QSAR models were externally validated by using LOO method to evaluate the predictivity of hypotheses [27, 28].

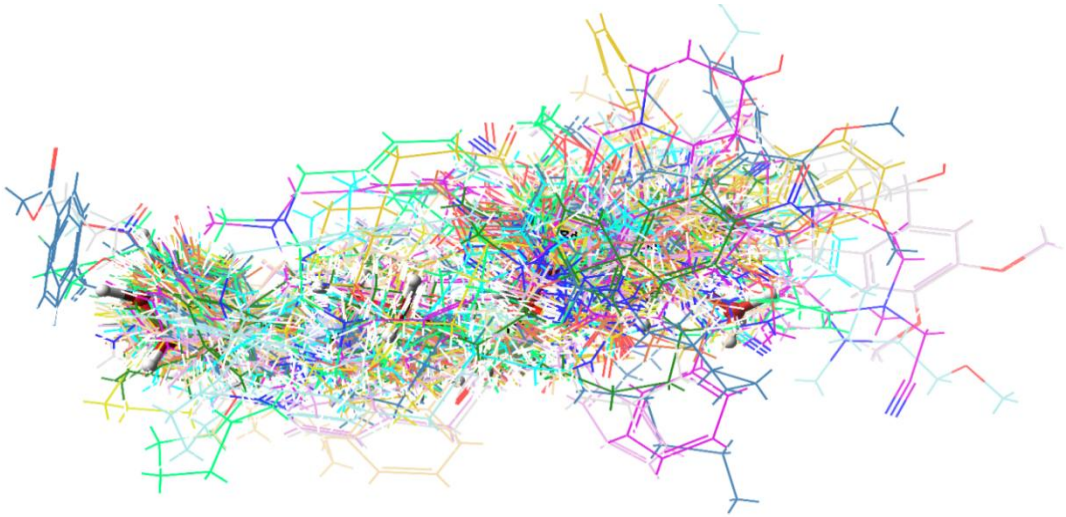

Figure 3.2 Alignment of all 142 AChE inhibitors with developed pharmacophore hypothesis.

3.2.4 Energy-optimized structure-based pharmacophore generation

Out of total 15, three X-ray crystal structures of hAChE with good resolution and PAS site AChE inhibition activity of cocrystal ligand, were collected from Protein Data Bank (https://www.rcsb.org). The cocrystal ligands of three PDB structures *viz.* 4EY7 (donepezil, IC_{50} 5.3 nM), 4M0E (dihydrotanshinone I, Ki 700 nM), and 4M0F (territrem B, IC_{50} 7nM, & Ki 1.7 nM) are shown in **Figure 3.3**.

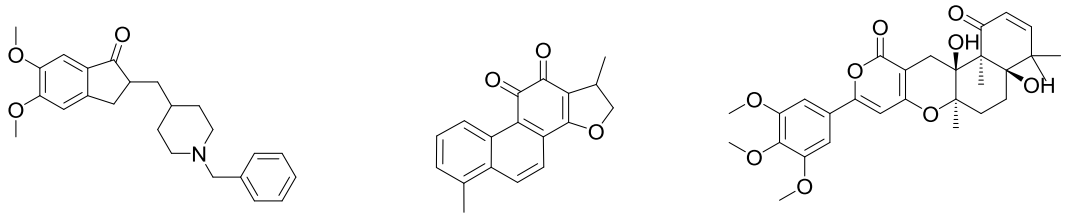

Figure 3.3 Structures of cocrystal ligand with PDB id and resolution.

Protein structures were prepared using protein preparation wizard in Maestro 10.1 with an OPLS_2005 force field. The Grids of all three PDB structures were prepared at the center of cocrystal ligand using receptor Grid Generation tool in Maestro 10.1. The

refined crystal ligands were docked by utilizing Glide XP (extra precision) docking with corresponding protein structures. The Glide XP energy was ranked by their contribution to the binding of pharmacophoric sites to cocrystal ligand [29]. PHASE v4.2 was applied to generate pharmacophore features, based on XP energy descriptor information. It was used to develop pharmacophore sites *viz.* H-bond acceptor (A), H-bond donor (D), hydrophobic group (H), negative ionizable group (N), positive ionizable group (P), and aromatic ring (R). H-bond acceptor and H-bond donor were pointed as vectors, directed to corresponding H-bond donor and acceptor positions at the binding site of receptors respectively. The Glide XP descriptors consisted of hydrophobic enclosure, hydrophobically packed associated hydrogen bonds, electrostatic rewards, π-π stacking, π-cation, and other interactions. Most favorable sites were selected for the development of e-pharmacophore hypothesis by using excluded volume.

3.2.5 Energy-optimized structure-based pharmacophore validation

Enrichment factor (EF) and goodness of hit (GH) were calculated to validate e-pharmacophore hypotheses (equation **2.1** and **2.2** respectively). A dataset of compounds was prepared using known actives of 53 AChE inhibitors (inhibitors with IC_{50} less than 100 nM and out of molecules utilized for the 3D-QSAR model). The data set included 1000 drug-like decoys (http://www.schrödinger.com/glide_decoy_set) with an average molecular weight of 400 D (the “dl-400” dataset) to validate e-pharmacophore models. LigPrep with Epik was applied to prepare database ligands with an OPLS_2005 force field. EF is the fraction of known actives retrieved after a screening of decoy database compounds [30].

3.2.6 Pharmacophore-based screening of the database

Only ‘hit-like’ compounds with unknown AChE inhibitory effect were collected from ‘ZINC15’ database utilizing Lipinski’s filter. LigPrep with Epik was employed to prepare database ligands utilizing OPLS_2005 force field. One ligand-based pharmacophore and three e-pharmacophore based matched molecules were separately screened against prepared database compounds with PHASE v4.2 [31]. Pharmacophore matching was required for the most energetically favorable site, and score of more than 1.0 kcal mol^{-1} was selected. For the pharmacophore screening, four sites for hypotheses with three or four, and five sites for hypotheses with four or five were required to match. The tolerance of distance matching was set to 2.0 Å. The aligned conformer of molecule matches the hypothesis based on rmsd, site matching, vector alignments, and volume terms expressed as fitness score [32]. The pharmacophore matched database was ranked in order of the fitness score ranging from 0 to 3, as applied in the PHASE. The ligands were selected up to 2000 molecules based on highest fitness scores for each pharmacophore and scores above 1.5 were considered as suitable inhibitor. The molecules with best fitness score were docked into the binding sites of AChE crystal structure [29].

3.2.7 Removal of pan-assay interference compounds

Baell and Holloway reported a list of structural features, which generated frequent false positives across screening, known as PAINS [24]. Jasial S. *et al.*established a large-scale analysis of behavior of PAINS in biological screening assays [33]. The PAINS free ‘ZINC15’ database molecules categorized within (A) anodyne, and (B) clean (PAINS-ok) [34], used in the earlier study, were selected as hits from HTVS retrieves. Other details have been included in Chapter 2, Section 2.2.8.

3.2.8 High throughput virtual screening and molecular docking

Glide HTVS (high throughput virtual screening) is faster than Glide SP and XP, has higher tolerance to suboptimal fits than Glide XP and thus is selected for the study [30]. After removal of PAINS, e-pharmacophore matched compounds were docked into binding sites of respective crystal structures, and ligand-based matched molecules were docked into 4M0E structure with Glide in Maestro [35]. The grid was generated at the center position of cocrystal ligand, through Grid Generation tools in Glide. Post-docking MM-GBSA minimization was performed to optimize the ligand geometries. The Glide HTVS screened molecules, with best docking scores, were selected for Glide SP, and XP screenings. Top 10% of retrieves, out from each step, were taken up for next step. Finally, all the non-peptide retrieves from HTVS and donepezil were docked in Glide XP molecular docking using 4M0E crystal structure (highest resolution PDB with cocrystal ligand, 2.0Å) to compare the docking score of screened out retrieves with reference donepezil.

3.2.9 Induced fit docking

A mixed molecular docking and dynamics method are known as induced fit docking (IFD) [36] was applied, where the receptor was flexible (in docking study). After ADME screening, selected hits were prepared by OPLS_2005 force field utilizing LigPrep. The hits were docked to rigid protein by using Glide in Maestro with scaling of ligand Van der Waals (vdW) radii 0.5 for nonpolar atoms [37]. Constrained energy minimization was performed on AChE (PDB: 4M0E) crystal structure, keeping it close to the original crystal structure, while removing bad steric contacts. The energy minimization of protein structure was performed using OPLS_2005 force-field. The Glide XP was utilized for initial docking, and 20 ligand poses were retained for protein structural refinement. Prime, Schrödinger 2015-1 was used to refine residue within 5.0Å

of ligand poses and to generate the induced-fit protein-ligand complexes. Each of the 20 complexes was subjected to refinements of side-chain and backbone [37] and was ranked according to Prime energy. The receptor structures within 30 kcal mol^{-1} were redocked for final round of Glide docking and scoring. The Prime refinement included at least one atom of all residues located within 4.0 Å of corresponding ligand pose. In the last step, every ligand was redocked into each refined low-energy receptor structure generated in the refinement step. The new 20 receptor conformations were taken forward for Glide XP redocking. The binding affinity of each complex was reported in the Docking Score. The more negative Docking Score indicates more favorable binding with receptor.

3.2.10 Docking using Autodock

AutoDock Tools-1.5.6 and AutoDock 4.2 suite were used to redock the selected hits as AChE inhibitor, for comparison of Glide XP docking, IFD, and AutoDock results. AChE crystal structure, 4M0E, was prepared using AutoDock Tools. Atom charges, solvation parameters, and polar hydrogens were added to enzyme structure for docking simulation before applying to PDBQT file format. The Chem3D 16.0 chemical structure drawing software was utilized to draw hits with standard 3D structures and to minimize energies of the compounds using MM2 energy minimization method [42]. The AutoDock 4.2 ligand optimization was performed using Gasteiger charges optimization, non-polar hydrogens were merged, and saved as PDBQT file. AutoDock required pre-calculated grid maps, and the grid must surround the region of active site of AChE. Therefore, the grid box was centered at the active site including Leu289, Arg296, Phe297, Phe338, Trp286, Ser293, Val294, Phe295, Tyr72, Tyr341, Asp74, Tyr124 and Tyr337 amino acid residues. The grid box size was positioned at 40, 42, and 48Å and the grid center was set to 20.683, −16.615, 19.006 for x, y and z respectively, covering

the active pocket. AutoGrid 4.0 was used to produce a grid with 0.375Å spacing between grid points. The Lamarckian Genetic Algorithm (LGA) was used to search best conformers, and a maximum of 50 conformers was considered for each compound with the default setting. The Discovery Studio Visualizer was used for visualization of interactions. AutoDock Tools provided various methods for analyzing the results of docking simulations, *viz.* conformational similarity, visualization of binding site and its energy, intermolecular energy, and inhibition constant.

3.2.11 Prime MM-GBSA simulation

The free binding energies of highest scoring docked complexes were computed by utilizing molecular mechanic-generalized Born surface area (MM-GBSA) [38], followed by default parameters. Based on the docking score and MM/GBSA binding-free energy, Jin *et al.* developed correlation model between docking scores or calculated binding-free energies and experimental pIC_{50} values [39]. The Prime in Maestro v10.1 was employed to calculate the MM-GBSA energy of Glide XP docked complex. The OPLS_2005 force field in conjunction with GBSA continuum model [40] was utilized to determine energies of selected complexes of ligands. Computationally, the binding free energies (ΔG_{bind}) of ligands were calculated using the equation **2.3** and **2.4** [41] (Chapter 2, Section 2.2.11).

3.2.12 ADME properties prediction

The QikProp in Maestro 10.1 [43] was used to predict ADME properties of hit molecules. As QikProp was unsuitable for neutralizing the compounds and generating the descriptors in the normal mode; hence, neutralization of all molecules was essential before performing QikProp. The QikProp predicted physicochemically significant and pharmaceutically applicable 44 descriptors for the hits. These included principle descriptors, physiochemical properties as well as log P (octanol/water), QP%, log

HERG, Caco-2 cell membrane permeability, MDCK cell permeability, skin permeability log Kp and Lipinski's rule of five, which were crucial for rational drug design [44, 45].

3.2.13 Density functional theory

Density functional theory (DFT) is utilized to determine and validate enzymatic reaction mechanisms and enzyme active sites. Electronic effects of drug-like compounds play an essential role in pharmacological effects [46]. Most and least active AChE inhibitors of training set were optimized with the final hits in Jaguar v8.7 (Schrödinger, LLC, New York, NY, 2015) program utilizing Lee-Yang-Parr correlation functional (B3LYP) theory, and Becke's three-parameter exchange potential [47, 48] with 6-31G* basis set. The molecular orbital surfaces, atomic electrostatics potential charges (EPS) and molecular electrostatic potential (MESP) were determined to calculate the HOMO and LUMO. The HOMO energy of small ligand molecules can donate electrons during the drug-enzyme complex formation, while LUMO energy manifests the capacity of the molecule to accept the electrons from the protein. HOMO-LUMO gap energy (difference in HOMO and LUMO energy), expresses electronic excitation energy, that is essential to compute the molecular reactivity and stability of drug-protein complex [49].

3.2.14 *In silico* AChE selectivity study

The XP docking of hits was carried out by using crystal structure of 4BDS (highest resolution PDB of human BuChE, 2.1 Å) to determine binding affinity of hits towards BuChE. The Glide in Maestro was used to perform Glide XP docking in default setting for all docking steps, and the Grid was centralized at the PAS site of BuChE, *i.e.*, centralized the residues ASp70, Trp 82, Asn83, Ser198, and Tyr332 [50].

3.2.15 *In vitro* AChE and BuChE enzyme inhibition

Four selected hit molecules out of ten (ZINC20592007, ZINC05354646, ZINC20649934, and ZINC39154782), were purchased from MolPort SIA, Riga, Latvia (MolPort id: MolPort-002-672-705, MolPort-002-658-497, MolPort-005-915-644, and MolPort-004-876-009 respectively). The AChE and BuChE inhibition were performed by modified Ellman *et al.* method [33] and the detail methods have been illustrated in Chapter 2, Section 2.2.17.

3.2.16 Assay of propidium iodide displacement

Propidium iodide is a PAS selective ligand, which displays 10-fold fluorescence enhancement on binding with AChE. Its dislocation by hits is measurement of their affinity to PAS of AChE and the methods have been described in Chapter 2, Section 2.2.18.

3.2.17 *In vitro* blood-brain barrier permeation assay

The *in vitro* blood-brain barrier (BBB) permeation of hits was predicted by parallel artificial membrane permeation assay (PAMPA) of BBB as described by Di L. *et al.* [51] and the procedure has been depicted in Chapter 2, Section 2.2.19.

3.2.18 Determination of cellular cytotoxicity and neuroprotection

MTT assay [52] was performed to establish cytotoxicity of selected hits and neuroprotectivity of hits was determined by evaluating their ability to protect SH-SY5Y cells against L-glutamate excitotoxicity-induced apoptosis (Chapter 2, Section 2.2.20).

3.2.19 Molecular dynamics simulation

MD simulations of the docked complex of ZINC20592007 (most active ligand of *in vitro* tests and 100% PAS selective), ZINC20649934 (*in silico* higher docking score and *in vitro* 58% PAS selective), and donepezil with 4M0E were performed by utilizing

Desmond v2.2, Schrödinger 2015-1 with the OPLS 2005 force field [12, 53]. The illustrated methods have been described in Chapter 2, Section 2.2.21.

3.3 Results and Discussion

3.3.1 Development of ligand-based pharmacophore model

Atom-based 3D-QSAR model was developed by using 142 datasets, which was divided into actives, inactives, and moderately actives. Total 163 hypotheses were generated and the best pharmacophore hypothesis, HPRRR, was selected on the basis of good survival activity (3.7), Survival-inactive Score (2.22), vector score (0.998), volume (0.862), selectivity (2.576), energy scores, best active alignment, and number of site matches (**Table 3.1**). Hypothesis HPRRR: one hydrogen-bond acceptor, one positive ionizable group, and three aromatic rings showed the highest survival score. The developed 3D-QSAR pharmacophore model was statistically, internally and externally, validated to exhibit reliable predictions. Randomly selected 100 compounds in the training set and 42 in the test set were initialized to generate 3D-QSAR model. The statistical parameters were obtained by 'leave one out' (LOO) method and partial least-square (PLS) analysis. HPRRR hypothesis showed better predictive ability with PLS factor 5 over than others (**Table 3.2**).

Table 3.1 The 3D-QSAR pharmacophore hypothesis with various scores

Hypothesis[a]	Survival score	Survival-inactive score	Site score	Vector score	Volume	selectivity
HPRRR	3.7	2.22	0.84	0.998	0.862	2.576

[a] H, hydrogen bond donor; P, positively ionizable group; and R, aromatic ring.

3.3.2 Validation of ligand-based pharmacophore model

At PLS factor 5, hypothesis HPRRR showed low SD value of 0.225, RMSE 0.409, and P value 1.13e-064, and higher R^2 0.961 for training set, and good Q^2 of 0.729; Person-R

0.857; F value 465.7 for the test set. Therefore, the model had good predictivity at PLS factor 5 and was taken for further pharmacophore-based screening of database molecules. Pharmacophoric features of 3D-QSAR hypothesis are sketched in **Figure 3.4**. The distance between pharmacophores was within the range of 2.174–11.329 Å (**Table 3.3)**. All the parameters for external validation of ligand-based pharmacophore model helped to select best model (**Table 3.4**). The correlation coefficient (r^2) value of 0.922, cross-validation coefficient (r^2_{cv}) value 0.919, square of correlation coefficient value using the LOO method, ($R_m{}^2_{(LOO)}$), of 0.834, also helped to consider 3D-QSAR model as a better predictive model. The slopes of regression lines through origin (K and K′ value) and substantial values of correlation coefficients ($R_0{}^2$ and $R'_0{}^2$) were obtained from observed activity versus predicted activity plots (**Figure 3.5**). The values were also within limits and encouraged the model predictivity.

Table 3.2 PLS statistics for internal validation of hypothesis HPRRR

PLS factor	SD[a]	R^{2}[b]	F[c]	P	Stability	RMSE[d]	Q^{2}[e]	Pearson-R[f]
1	0.735	0.570	129.7	1.204e-019	0.933	0.651	0.314	0.588
2	0.482	0.817	216.5	1.706e-036	0.843	0.480	0.627	0.797
3	0.376	0.890	257.8	8.733e-046	0.770	0.468	0.646	0.813
4	0.288	0.936	347.5	8.721e-056	0.702	0.437	0.691	0.834
5	0.225	0.961	465.7	1.13e-064	0.678	0.409	0.729	0.857

[a]Standard deviation of the regression; [b]The square of correlation coefficient; [c]Variance ratio; [d]Root-mean-square error; [e]Squared Q value for the predicted activities; [f]Correlation between the predicted and observed activities for the test set.

3.3.3 Development of energy-optimized structure-based pharmacophore

Total three human AChE (hAChE) crystal structures with resolution between 2.0 Å and 2.35 Å and potent AChE inhibitory activity (IC_{50} between 5.3 to 7 nM and Ki 1.7 to 700 nM) were selected for developing e-pharmacophore. Protein preparation wizard was used to prepare the proteins with an OPLS_2005 force field. After refinement, the

protein structures with ligand interaction showed that donepezil (cocrystal of 4EY7) interacted with Trp86, and TRP286 by pi-pi stacking, H-bond with Phe295, and pi-cationic with Phe338 residue. The dihydrotanshinonr I (cocrystal of 4M0E) interacted with TRP286 by a pi-pi stacking, H-bond interaction was with Phe295; and territrem B (cocrystal of 4M0F) interacted with TRP286 by a pi-pi stacking and H-bond interaction was with Tyr124 at the PAS site (**Figure 3.6)**. The refined cocrystal ligands were redocked onto the respective prepared protein structures to generate energy-optimized structure-based pharmacophore (e-pharmacophore). The root-mean-square deviation (rmsd) was less than 1 Å for all three cocrystal ligands.

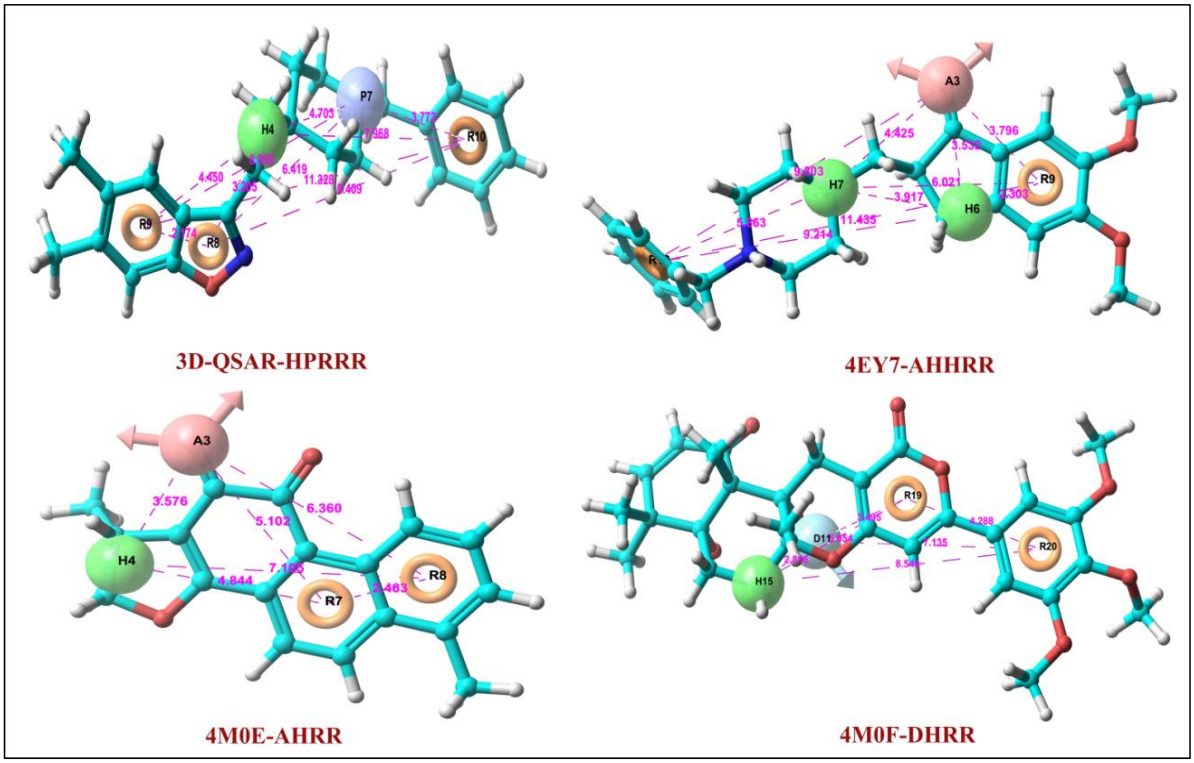

Figure 3.4 3D-QSAR pharmacophore hypotheses and structure-based pharmacophores models with their respective crystal structures. A, H-bond acceptor, Pink sphere containing arrow; D, H-bond donor, sky blue sphere with arrow; H, hydrophobic group, green sphere; P, positive ionizable group, violet sphere; R, aromatic ring, yellow circle.

The e-pharmacophore hypotheses were generated by mapping Glide XP energetic terms onto pharmacophore sites, which were calculated from the structural and energy information between protein and ligand. Initially, the number of pharmacophore sites

was set up to 10 for each crystal structure for pharmacophore generation. But number of pharmacophore sites was selected, for the best hypothesis, on the basis of validation parameters. The total number of pharmacophore sites for each cocrystal ligand, before energy-based site selection and selected sites, for hypothesis generation of three crystal structures with pharmacophoric feature scores are given in **Table 3.5**.

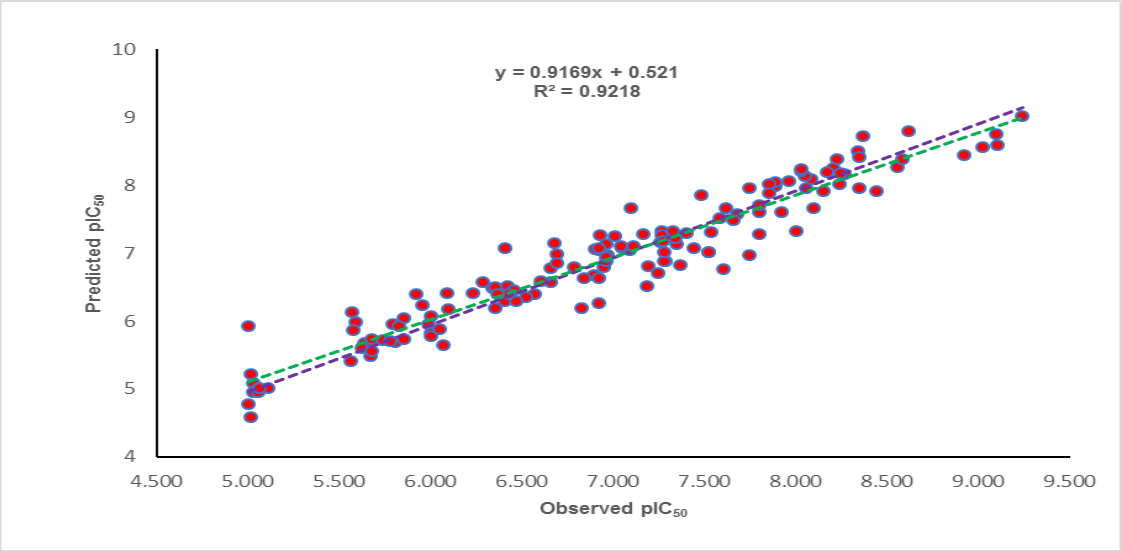

Figure 3.5 Plot of predicted pIC_{50} versus observed pIC_{50} of AChE inhibitors developed by model HPRRR with regression lines (original regression lines represented in green break line and regression lines with intercept zero in purple break line).

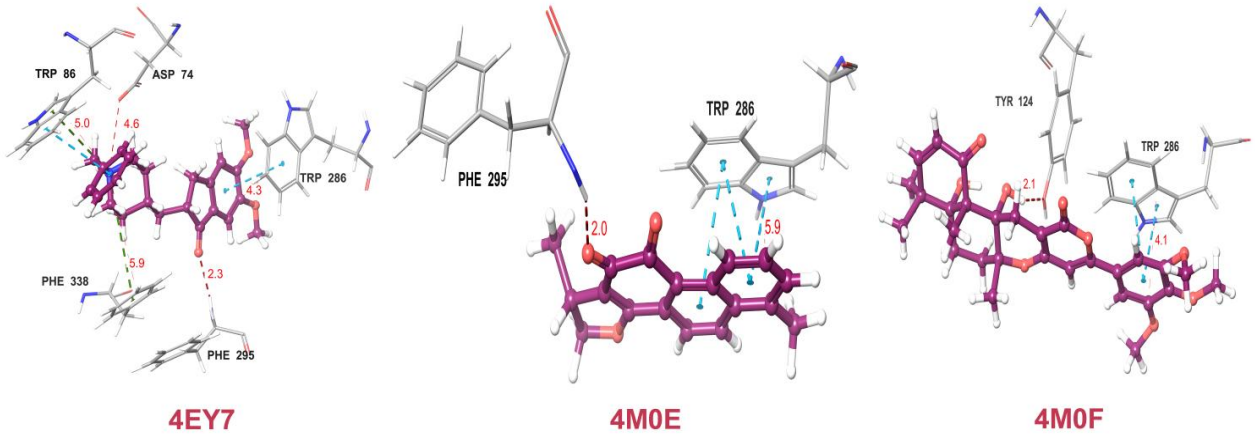

Figure 3.6 Crystal structures of AChE with cocrystal ligands (purple) and bonding interactions

The e-pharmacophore models generated were AHHRR with 5 sites from 4EY7, AHRR with 4 sites from 4M0E, and DHRR with 4 sites from 4M0F crystal structure (**Figure**

3.4). In these pharmacophore modelings, A strands for H-bond acceptor, D for H-bond donor, H for hydrophobic group, R for aromatic ring. The distance between e-pharmacophore features was within the range of 2.303–11.435 Å (**Table 3.3**).

Table 3.3 Distance between features of 3D-QSAR hypotheses and e-pharmacophores

Model[a]	**Distance from A to H (Å)**	**Distance from A to R (Å)**	**Distance from H to H (Å)**	**Distance from H to P (Å)**	**Distance from H to R (Å)**	**Distance from P to R (Å)**	**Distance from R to R (Å)**	**Distance from D to H (Å)**	**Distance from D to R (Å)**
3D-QSAR-HPRRR				4.703	3.205, 4.45, 7.968	6.419, 8.05, 3.773	2.174, 9.409, 11.328		
4EY7-AHHRR	3.532, 4.425	3.796, 9.803	3.917		2.303, 9.214, 6.021, 5.863		11.435		
4M0E-AHRR	3.576	5.102, 6.36			4.844, 7.105		2.463		
4M0F-DHRR					5.054, 8.549		4.288	2.816	3.495, 7.135

[a]Type of model written with pharmacophores; PDB used for the respective e-pharmacophore model.

Table 3.4 External validation parameters for 3D-QSAR

External validation parameter	**HPRRR**	**Limit**
r^2_{cv} [a]	0.919	$r^2_{cv} > 0.5$
r^2 [b]	0.922	r^2 close to 1
k value[c]	0.990	$0.85 \leq k \leq 1.15$
k´ value[d]	1.008	$0.85 \leq k \leq 1.15$
R_0^2 [e]	0.916	Close to r^2
$R_0'^2$ [f]	0.921	Close to r^2
$R_m^2{}_{(LOO)}$ [g]	0.834	$R_m^2{}_{(LOO)} > 0.5$
r^2_{pred} [h]	0.738	$r^2_{pred} > 0.5$

[a]Cross-validated coefficient; [b]Correlation coefficient between actual and predicted values; [c], [d]Slope values of regression lines; [e],[f]Correlation coefficients for regression lines through origin; [g]Modified squared correlation coefficient using LOO method; [h]Predictive correlation coefficient value.

3.3.4 Validation of energy-optimized structure-based pharmacophore

The database of 1053 compounds using 1000 drug-like decoys and 53 known AChE inhibitors, was utilized for e-pharmacophore validation. Enrichment factor (EF) and Goodness of hit score (GH) were evaluated by Güner-Henry scoring method to validate the e-pharmacophores (**Table 3.6).** The values of GH over 0.5 and EF higher than 10, ensured the suitability of pharmacophores for further pharmacophore-based virtual screening.

Table 3.5 e-Pharmacophore hypotheses with features scores

PDB	No. of possible site	No. of accepted site	Hypothesis[a]	Pharmacophore features with score
4EY7	6	5	AHHRR	H7: −1.64, H6: −1.5, R10: −1.48, R9: −1.2, A3: −0.73
4M0E	4	4	AHRR	A3: −1.7, R7: −1.62, H4: −1.5, R8: −1.13
4M0F	7	4	DHRR	R19: −1.5, D11: −1.49, R20: −1.3, H15: −0.66

[a]A, H-bond acceptor; D, hydrogen bond donor; H, hydrophobic group; P, positively ionizable group; R, aromatic ring

Table 3.6 Validation of e-pharmacophores with the Güner-Henry scoring method

Parameter*	4EY7	4M0E	4M0F
Ht[a]	74	69	71
Ha[b]	41	37	43
EF[c]	11.008	10.654	12.033
GH[d]	0.589	0.558	0.639

[a]Total Hits; [b]Active Hits; [c]Overall enrichment factor; [d]Goodness of hit score, *Parameters calculated using a dataset consisting of total 1053 compounds with 53 total actives compounds.

3.3.5 Pharmacophore matched screening and removal of pan-assay interference compounds

Pharmacophore matched molecules were separated from the total 3530990 ZINC15 database compounds (without known AChE inhibitors) by advance pharmacophore screening option of PHASE. The fitness value is a measure of how well the ligand fits

with the pharmacophore. The hits with high fitness value of over 1.5 are probably very active inhibitors. We employed the validated three e-pharmacophores, and one ligand-based pharmacophore to screen the database of 2000 AChE inhibitor molecules by each model. The reactivity towards proteins to develop poor potentiality or known toxicity of molecules, *i.e.*, PAINS was removed from pharmacophore matched compounds by RDKit, ZINC, and FAF-Drugs4 server (Appendix, **Table A.3**). Only less than 1% of PAINS compounds were removed, and mild PAINS were ignored for virtual screening.

3.3.6 High throughput virtual screening and molecular docking

High throughput screening of PAINS removed pharmacophore matched database was a fruitful resource for initial hit identification. The numbers of hits from pharmacophore-based virtual screening and selection process with their respective PDB are presented in **Table 3.7**. Molecular XP docking was performed for all the outcome HTVS retrieves with 4M0E crystal structure to compare docking scores of hits with reference donepezil. Total 55 molecules were having docking score of more than −9.0. Finally, eight compounds with structural diversity, PAINS free (except ZINC20592007, a PAINS-ok molecule), better docking scores (−12.87 to −10.74) and Glide energies (−56.48 to −42.16 kcal mol^{-1}) than donepezil were selected for further studies (**Table 3.8**). The hits outcome concerning pharmacophore models is listed in **Table 3.9**.

Table 3.7 Number of compounds retrieved at each stage of screening of dataset

Pharmacophore model	PDB	HTVS hits	SP hits	XP hits	No. of selected hit(s)
AHHRR	4EY7	1991	200	20	1
AHRR	4M0E	1873	199	19	2
DHRR	4M0F	1993	200	20	2
HPRRR	4M0E	1945	200	20	3

Table 3.8 Hits with their Glide docking score, number of H-bonds, interaction with essential amino acids, IFD docking score, and AutoDock binding energy

Compound	Glide docking score (AChE)	Glide docking score (BuChE)	H-bond	Glide energy	Residue interactions	MM-GBSA-ΔG_{Bind}	IFD docking score	AutoDock binding energy
ZINC72451013	−12.87	−6.52	3	−51.63	Asp74[c], Phe295[d], Arg296[d], Tyr337[d], Tyr341[a]	−65.17	−11.53	−10.34
ZINC20649934	−12.65	−5.85	2	−50.50	Asp74[c], Trp286[a], Phe295[d], Tyr337[d], Tyr341[b]	−94.16	−10.77	−11.69
ZINC05354646	−11.93	−5.66	1	−42.16	Trp286[a],[b], Phe295[d]	−73.30	−12.64	−9.85
ZINC79331983	−11.40	−8.78	4	−54.98	Asp74[d],[d], Phe295[d], Tyr337[d]	−79.39	−11.09	−10.65
ZINC20592007	−11.26	−8.5	2	−47.79	Tyr72[d], Trp286[a], [b], His287[a], Phe295[d]	−79.10	−12.78	−10.77
ZINC77161317	−11.02	−7.31	1	−51.02	Trp286[b], Phe295[d], Phe297[a]	−69.09	−12.699	−9.75
ZINC58160603	−10.93	−7.35	1	−49.16	Trp286[b], Phe295[d]	−80.61	−11.85	−9.32
ZINC39154782	−10.74	−9.34	3	−49.28	Asp74[c], [d], Try124[a], Ser293[d], Tyr337[a], [d], Tyr341[b], Phe297[a], Phe338[a]	−76.11	−11.88	−10.54
Donepezil	−8.24	-	1	−43.89	Tyr124[b], Trp 286[a], Phe295[d], Phe 338[b]	−62.30	−8.91	−9.64

[a] Pi-Pi stacking; [b] Pi-cation interaction; [c] Salt bridge; [d] H-Bond interaction

The protein-ligand interactions with types of interactions and interacting residues with hits and donepezil are included in **Table 3.8**. The chemical structures of hits are

sketched in **Figure 3.7** and ligand-protein interactions are pictured in **Figure 3.8**; hits are represented in yellowish green, interacting amino acid residues of protein in gray, H-bond in red, pi-cationic interaction in green and pi-pi stacking in cyan.The presence of more hydroxyl, keto, secondary amine and nitrogen-containing hetero aromatics in hits were responsible for formation of hydrogen bonds and better docking scores than donepezil. The hits mainly bind at PAS site of AChE through H-bond interactions with Phe295, Tyr337, and Phe338 residues (within 1.8–2.3 Å bond distance), pi-pi stacking with Trp286, His 287, Phe297, and Tyr341 residues (within 3.8–5.1 Å distance), and pi-cationic or salt bridge interactions with Asp74, Tyr341, and Trp286 residues (within 1.9–5.6 Å distance).Carbonyl group of ZINC77161317 and ZINC39154782 formed H-bonding with Phe295 and Ser293; whereas in rest of the hits, the group formed hydrogen bonding with Phe295 reside of protein. Aromatic group of hits produced π-π stacking interaction with Trp286, except ZINC39154782 which interacted with Phe297.

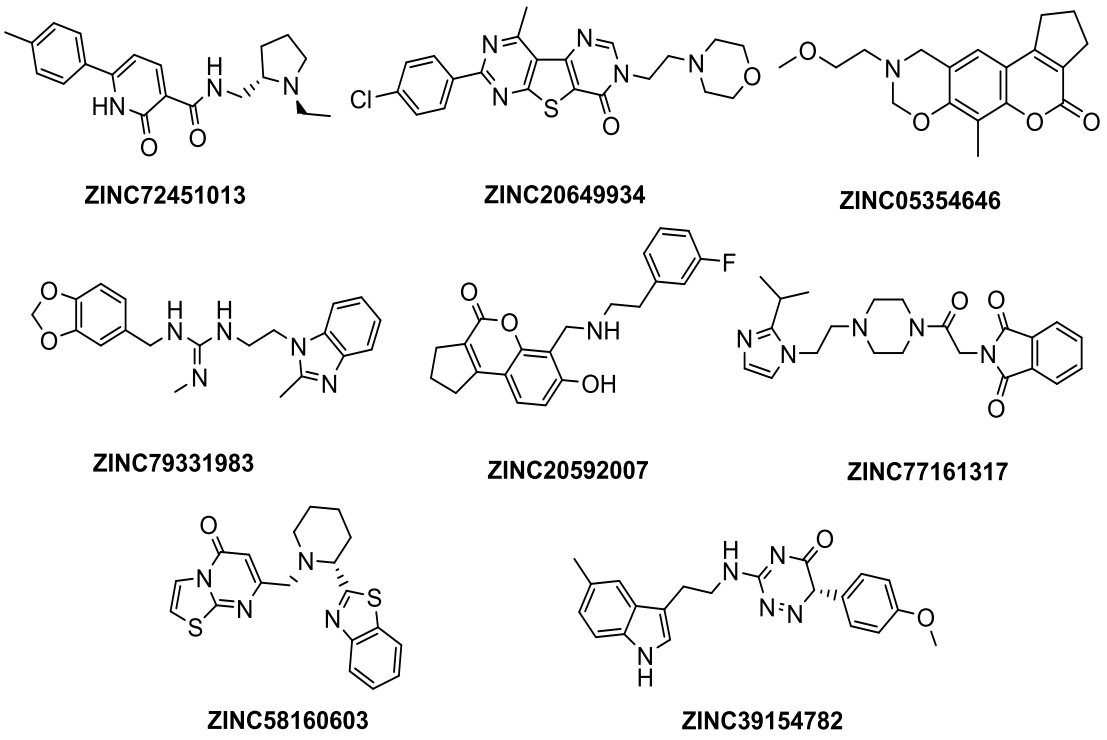

Figure 3.7 Structures of final selected hits with Zinc database ids.

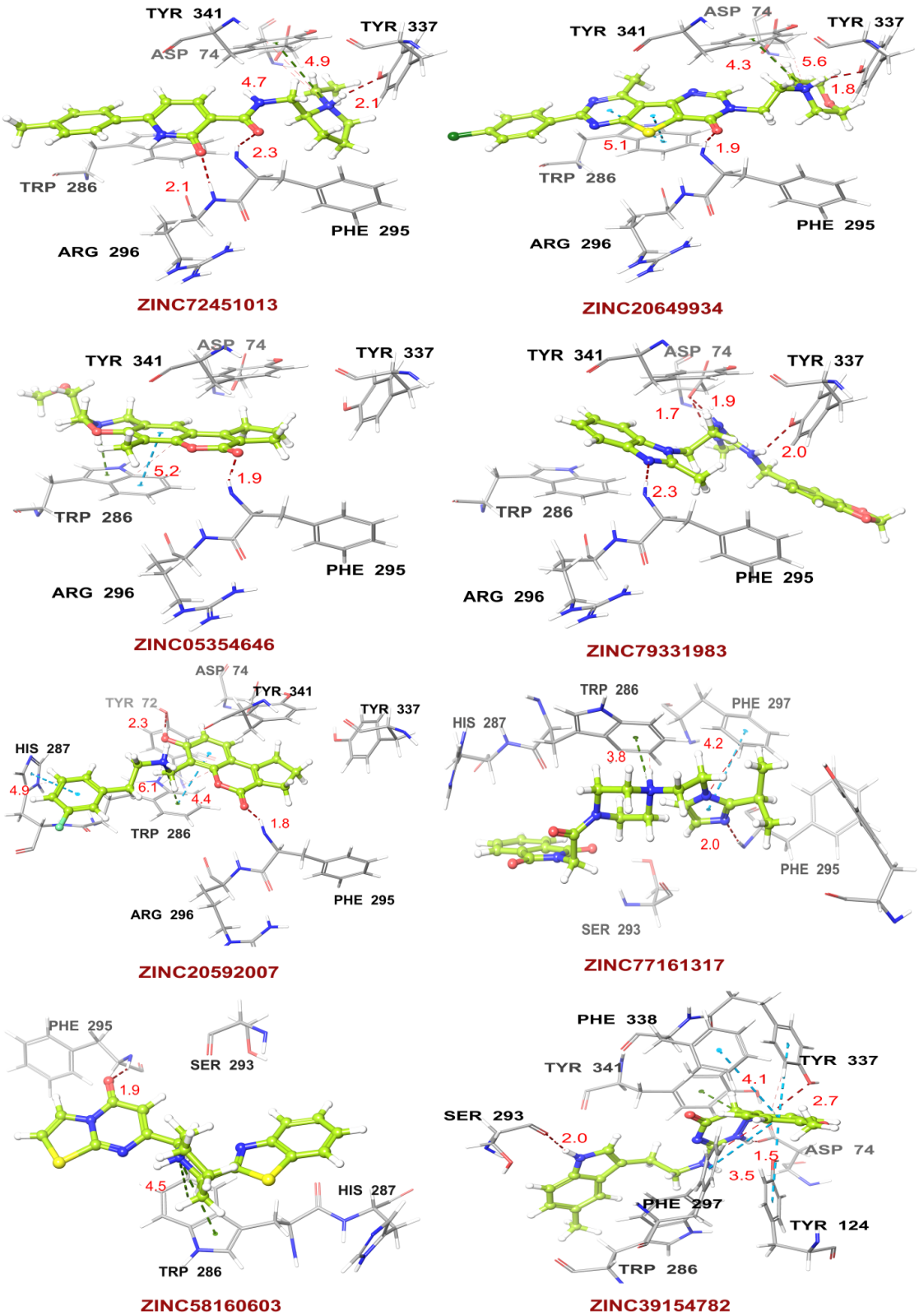

Figure 3.8 Docking poses of ZINC72451013, ZINC20649934, ZINC05354646, ZINC79331983, ZINC20592007, ZINC77161317, ZINC58160603, and ZINC39154782 with AChE crystal structure; hits represented in yellowish green, residues in gray, H-bond in red, pi-cationic interaction in green and pi-pi stacking in cyan.

Table 3.9 Final hits outcome from respective pharmacophore models

Hit	Pharmacophore model
ZINC72451013, and ZINC20649934	DHRR
ZINC05354646, and ZINC20592007	AHRR
ZINC79331983, ZINC58160603, and ZINC39154782	HPRRR
ZINC77161317	AHHRR

3.3.7 Induced fit docking

The IFD scores of hits were close to the Glide XP docking scores (**Table 3.8**). The conformations generated from the IFD were little different from the docked poses, produced from the rigid receptor docking. The Glide-based model provided an RMSD of 5.2Å as compared to the native pose in the crystal structure. The IFD docking pose and score were supported by the binding positions, affinity, and stability of hits.

3.3.8 Docking with AutoDock

Binding energy of final eight hits was between −9.32 to −11.69 kcal mol^{-1}. The prediction of results fully supported Glide XP docking and IFD results. All the hits displayed similar binding affinity and docking pose with 4M0E (**Figure 3.9** and **3.10**).

3.3.9 Calculation of Prime MM-GBSA

Prime MM-GBSA simulation was calculated for AChE-hits and AChE-cocrystal ligand complexes utilizing Maestro 10.1 (**Table 3.8**) to predict the binding mode and binding free energy (ΔG_{bind}). All the hits showed better ΔG_{bind}, with ZINC20649934 providing highest ΔG_{bind}, of −94.16 kcal mol^{-1}. The binding free energy, based on Prime MM-GBSA, established the stability of AChE-hit complexes.

3.3.10 Prediction of ADME properties

The prediction of drug-likeness and pharmacokinetics, including absorption, distribution, metabolism, and excretion (ADME) was performed on QikProp tools of

Maestro 10.1. Physiochemical descriptors and pharmaceutically relevant properties of hits were evaluated for their druggable properties (**Table 3.10**). All the hit molecules showed good partition coefficient (QPlogPo/w) values (1.6 to 3.854), which were critical for absorption and distribution of drugs. Factor QPPCaco, indicating permeability of these hits, was in the range of 79.257 to 1879.796, where QPPCaco was a predicted apparent Caco-2 cell permeability in nm/s value, a key factor for the estimation of cell permeability in biological membranes.

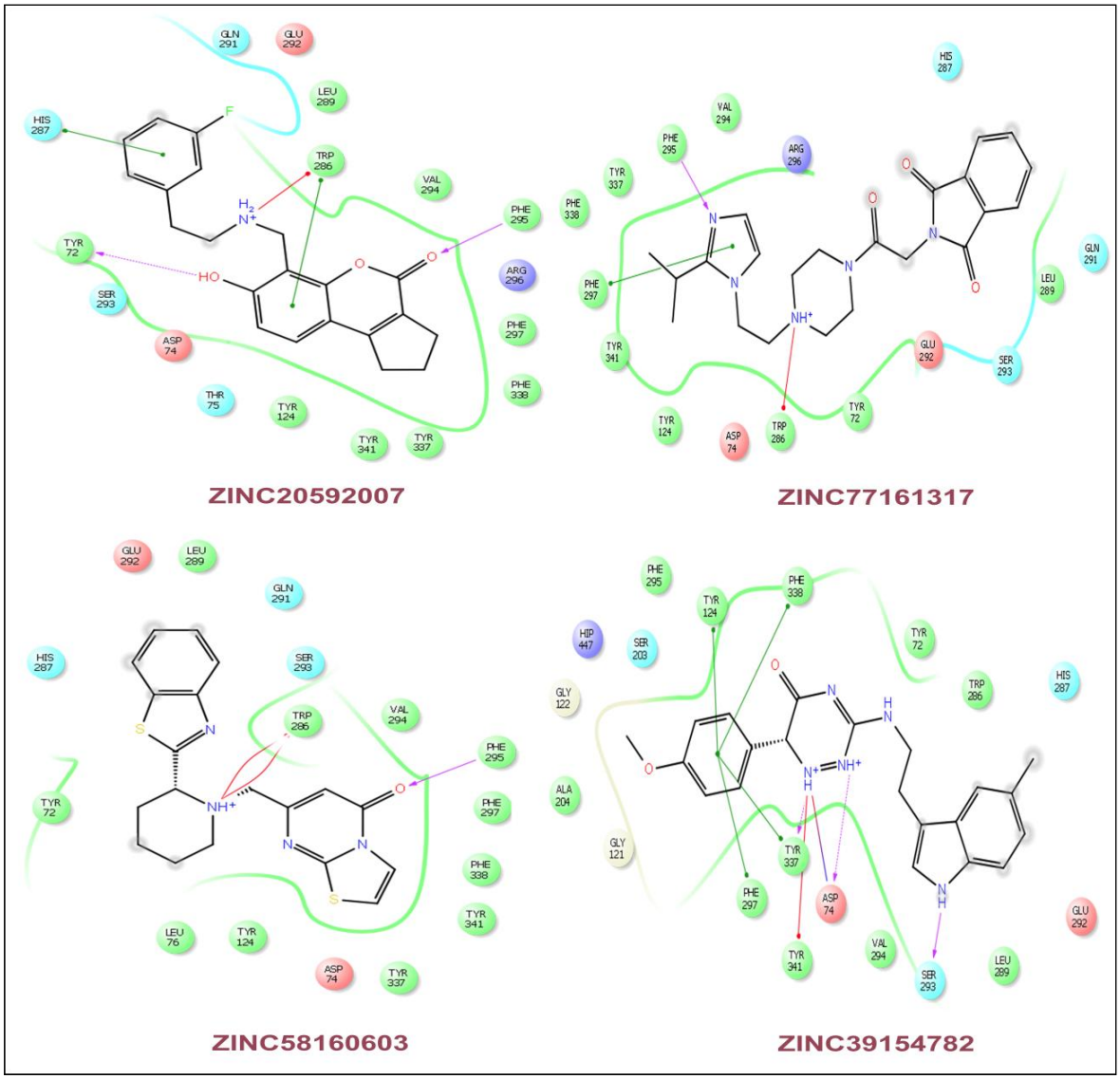

Figure 3.9 Docking pose of four hits with 4M0E crystal structure using AutoDock (purple arrow indicates H-bond; green line denotes π-π stacking; red line for pi-cationic interactions.

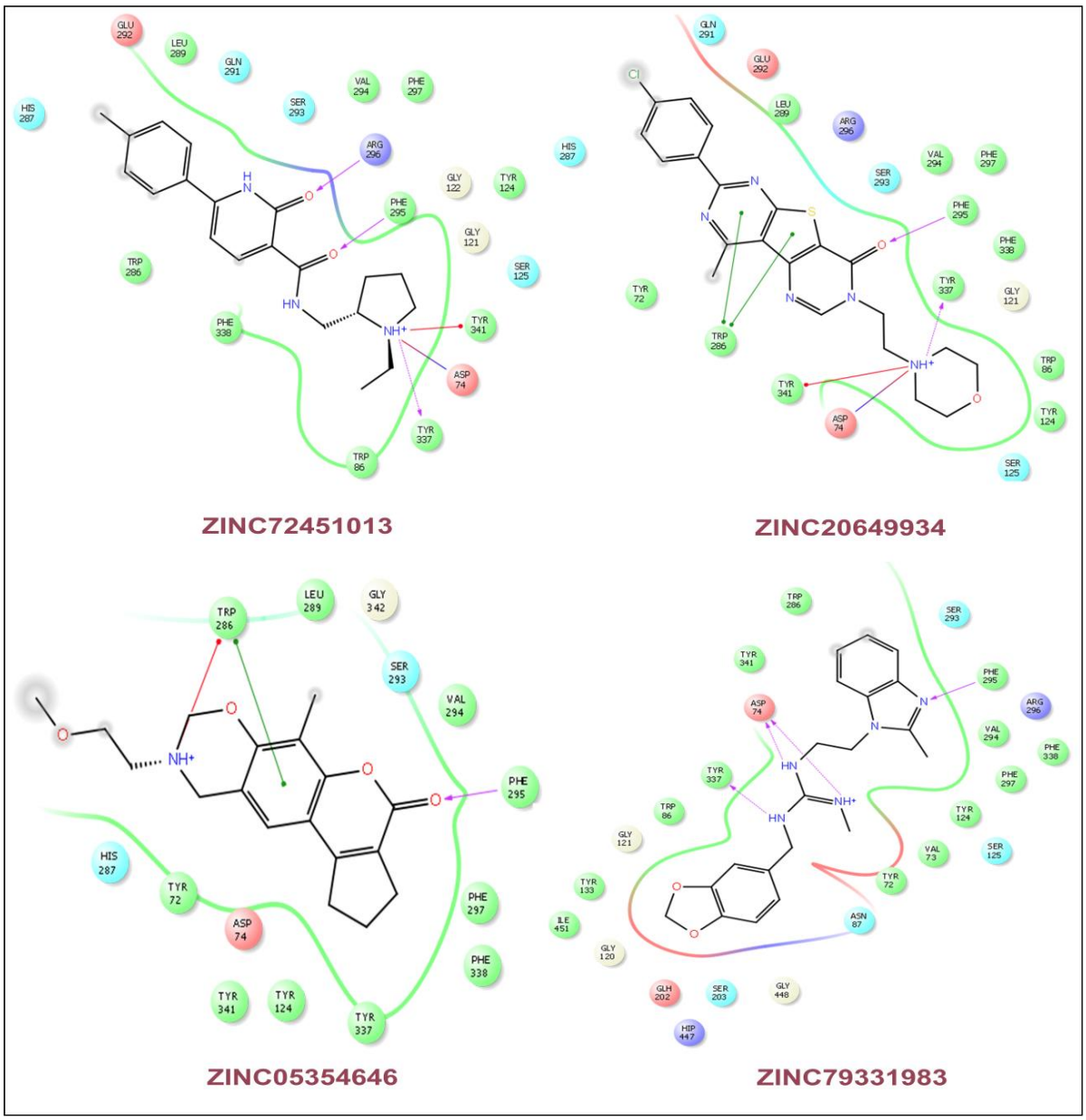

Figure 3.10 Docking pose of another four hits with 4M0E crystal structure using AutoDock (purple arrow indicates H-bond; green line denotes π-π stacking; red line for pi-cationic interactions.

The hits successfully passed entire pharmacokinetic requirements for a drug-like compound and were within the acceptable range as defined for human use. Overall, the percentage of human oral absorption for the hits was between 70.301 to 100%, their water solubility (QP log S) ranged between −1.919 to −6.373, pMDCK (cell-permeable parameter) values were between 56.117 to 1193.73, skin permeability (logKp) values were within −2.709 to −4.898; plogHERG (K^+-channel blockage) values were less than

−5 and hence were a concern. Additional parameters, *i.e.*, molecular weight, H-bond donors, H-bond acceptors, and logP according to Lipinski's rule of five, were also evaluated. Hits with better binding interactions and good predicted pharmacokinetic properties were considered for *in vitro* studies.

Table 3.10 Hit molecules and their physiochemical descriptors determined by Qikprop

Zinc15 id[a]	**QPlog Po/w[b]**	**QPlog S[c]**	**QPlog HERG[d]**	**QPPCaco[e]**	**QPP MDCK[f]**	**QPlogKp[g]**	**% Human oral absorption[h]**
ZINC72451013	3.586	−4.62	−6.76	249.141	121.859	−4.273	90.84
ZINC20649934	2.619	−3.37	−6.631	529.903	1193.73	−3.718	91.04
ZINC05354646	1.627	−1.92	−5.112	553.223	288.626	−4.359	85.56
ZINC79331983	3.854	−4.37	−5.055	1879.796	978.659	−3.407	100
ZINC20592007	3.448	−4.50	−6.75	199.231	173.105	−4.22	88.29
ZINC77161317	1.6	−2.38	−5.559	79.257	56.117	−4.617	70.30
ZINC58160603	2.674	−3.38	−6.619	393.786	546.198	−3.897	89.06
ZINC39154782	3.311	−5.64	−6.286	406.683	187.069	−2.709	93.04

Recommended values are: [a]Zinc database compound id; [b]QPlog Po/w for octanol/water (−2.0 to 6.5); [c]QPlog S: Predicted aqueous solubility, S in mol dm^{-3} (−6.5 to 0.5); [d]log HERG: HERG K+ channel blockage (<-5); [e]Apparent Caco-2 cell permeability (nm/s) (<25 poor, >500 great); [f]Apparent MDCK permeability (nm/s) (<25 poor, >500 great); [g]QPlogKp: skin permeability ; [h]% Human oral absorption (>80% is high and <25% is poor).

3.3.11 Density functional theory

HOMO and LUMO of chemical compounds are crucial indicators of their reactivity and stability of ligand-receptor interactions [49]. The stability of interactions is inversely correlated to energy gap between HOMO and LUMO orbitals. The orbital energy of all energetically stable hit molecules was calculated by DFT method. The high value of HOMO energy is likely to indicate the tendency of molecule to donate electrons to an appropriate acceptor molecule with LUMO. The correlation of HOMO energy with IC_{50} data suggested that the HOMO of inhibitor might transfer its electrons to less energy, LUMO, of some amino residues in the active site of the enzyme. The calculated DFT

properties of all hits are provided in **Table 3.11**. The HOMO-LUMO energy gap of hits was minimal, and between −0.182 to −0.012 eV. Lesser HOMO-LUMO energy gap facilitated electron(s) density exchanging properties or encouraged some interaction(s). The mean ESP indicated electron density distribution around nuclei of the molecules and was between −0.22 to 1.89 kcal mol^{-1}. ESP data indicated that most of the hits contained both low and high electron density sites in a molecule. The upper and lower electron density regions may correspond to the hydrogen bonding between the hits and enzyme.

3.3.12 *In silico* AChE selectivity study

Glide XP docking study against BuChE was performed 4BDS crystal structure to estimate selectivity of hits towards AChE. All the hits had BuChE binding affinity with more selectivity towards AChE (**Table 3.8**). The hit ZINC05354646 showed lowest Glide docking score (−5.66 kcal mol^{-1}), and next lowest score was of ZINC20649934 (−5.85 kcal mol^{-1}) against BuChE crystal structure, 4BDS. BuChE binding property of hits with AChE inhibition improved their therapeutic property for cholinergic activity.

Table 3.11 Calculated DFT properties of hit molecules

Hit	HOMO	LUMO	HOMO-LUMO gap	ESP mean (kcal mol^{-1})
ZINC72451013	−0.205	−0.069	−0.137	−0.13
ZINC20649934	−0.229	−0.079	−0.150	1.38
ZINC05354646	−0.215	−0.047	−0.168	1.51
ZINC79331983	−0.199	−0.021	−0.177	1.88
ZINC20592007	−0.218	−0.048	−0.171	0.96
ZINC77161317	−0.214	−0.078	−0.136	1.12
ZINC58160603	−0.222	−0.054	−0.168	−0.07
ZINC39154782	−0.20	−0.094	−0.105	−0.22

3.3.13 *In vitro* inhibition of AChE and BuChE

Four hits (ZINC20592007, ZINC05354646, ZINC20649934, and ZINC39154782), selected, on the basis of Glide docking score, AutoDock energy, AChE Selectivity, PAS site selectivity, ADME properties, and interesting structural features for further *in vitro* studies. ZINC20592007 contains 2,3-dihydrocyclopenta[c]chromen-4(1H)-one fused nucleus, which is PAINS-ok (mannich-A type) molecule. ZINC05354646, a 2,3,9,10-tetrahydro-8H-cyclopenta [3,4]chromeno[6,7-e][1,3]oxazin-4(1H)-one fused compound, is PAINS free with similar scaffold of ZINC20592007. ZINC20649934 has thieno[2,3-d:4,5-d']dipyrimidin-4(3H)-one nucleus with attached morpholine ring to ethylene linker. ZINC39154782 contains 1,2,4-triazin-5(6H)-one with indole ring attached through an ethyl amino linker (**Figure 3.7**).

The selected hits were evaluated for their anti-cholinesterase (anti-ChE) activity. AChE and BuChE inhibition activities were evaluated by the method described by Ellman [54], wherein donepezil was used as reference standard. Compound ZINC20592007 exhibited higher AChE inhibitory activity than ZINC05354646, ZINC20649934, and ZINC39154782 [IC_{50} values of 482±1.88, 580±1.63, 854±2.65, and 636±1.79 nM, respectively (**Table 3.12**)]. The hits have selective AChE inhibitory activity than BuChE enzyme (**Table 3.12**). The half maximal enzyme inhibitory concentration (IC_{50}), a measure of potency of hits inhibiting AChE and BuChE, was calculated by constructing a dose-response curve (**Figure 3.11**) by utilizing GraphPad Prism 5.0.

Mechanism of AChE enzyme inhibition of the four hits was determined by enzyme kinetic study. Lineweaver-Burk reciprocal plots were generated by plotting reciprocal of reaction rates and reciprocal of substrate concentrations using different concentrations of hit molecules. Velocity of AChE activity with varying concentrations of substrate (0.15–1.15 μM) in absence and presence hit molecules (0.25, 0.5 and 1 μM of

ZINC20592007 and ZINC05354646, and 0.5, 1, and 2 μM for ZINC20649934, and ZINC39154782) were calculated by Michaelis-Menten kinetics curve. The Ki values of hits were determined by Yonetani-Theorell method from Lineweaver-Burk plots and presented in **Figures 3.12**, **3.13**, **3.14**, and **3.15** for ZINC20592007, ZINC05354646, ZINC20649934, and ZINC39154782 respectively.

The plots revealed that increasing the concentrations of inhibitor result in an increase in slope (decreased V_{max}) and intercept (higher K_m). The lower value of V_{max} in Michaelis-Menten plot to increase, decrease, or leave unaffected apparent value of K_m, (**Table 3.13**) indicated non-competitive inhibition on the kinetic constants. The double reciprocal Lineweaver-Burk displayed a nest of lines that intersect at a point other than y-axis, and lines converge to the left of y-axis, and below the x-axis, *i.e.*, $\alpha < 1$, and indicating that the inhibitor binds with greater affinity to the enzyme-substrate (ES) complex or subsequent species. The calculated inhibitor constant (Ki) of hits (ZINC20592007, ZINC05354646, ZINC20649934, and ZINC39154782) were 0.21±0.027, 0.27±0.064, 0.3±0.018, and 0.28±0.032 μM respectively.

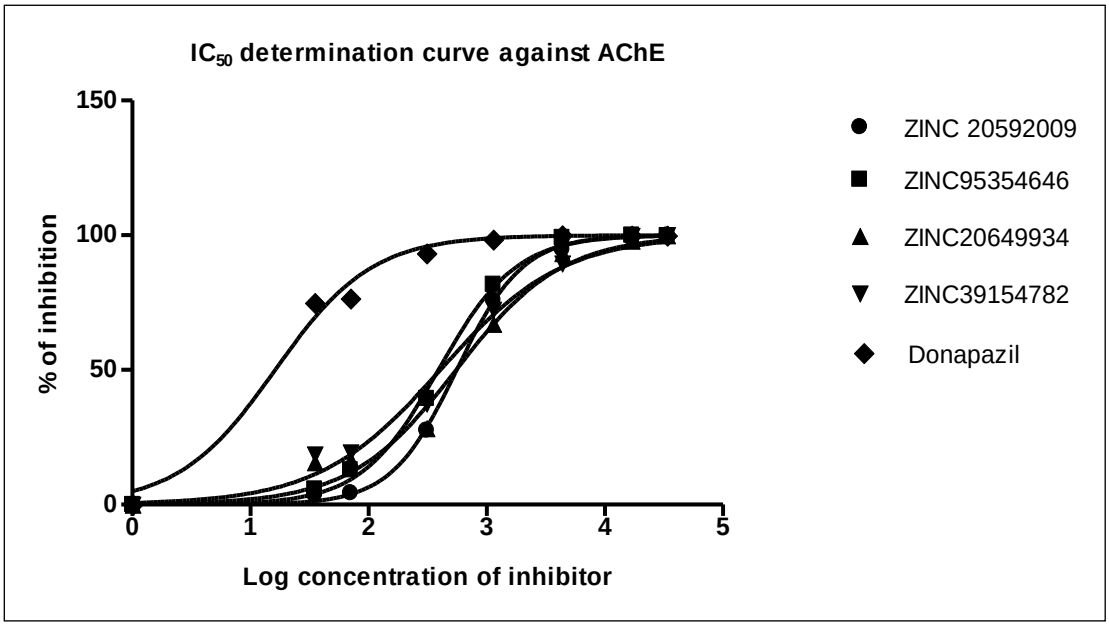

Figure 3.11 Dose-response curves of selected hits with donepezil.

Table 3.12. Inhibitory activity on AChE (electric eel), BuChE (horse serum) and propidium competition assay results

Compound	IC_{50} AChE (nM)[a]	IC_{50} BChE (nM)[a]	Selectivity[b]	Propidium displacement (%)		
				0.24 µM	1 µM	3 µM
ZINC20592007	482±1.88	23954±5.7	49.7	44	70	100
ZINC05354646	580±1.63	147424±6.7	254.2	0	42	57
ZINC20649934	854±2.65	148654±6.2	174.1	0	25	58
ZINC39154782	636±1.79	128064±5.1	201.4	29	58	100
Donepezil	24±0.29	7421±2.0	309.2	0	0	0

[a]Each assay was repeated three times independently; [b]Selectivity for AChE=[IC_{50} (BuChE)]/[IC_{50} (AChE)].

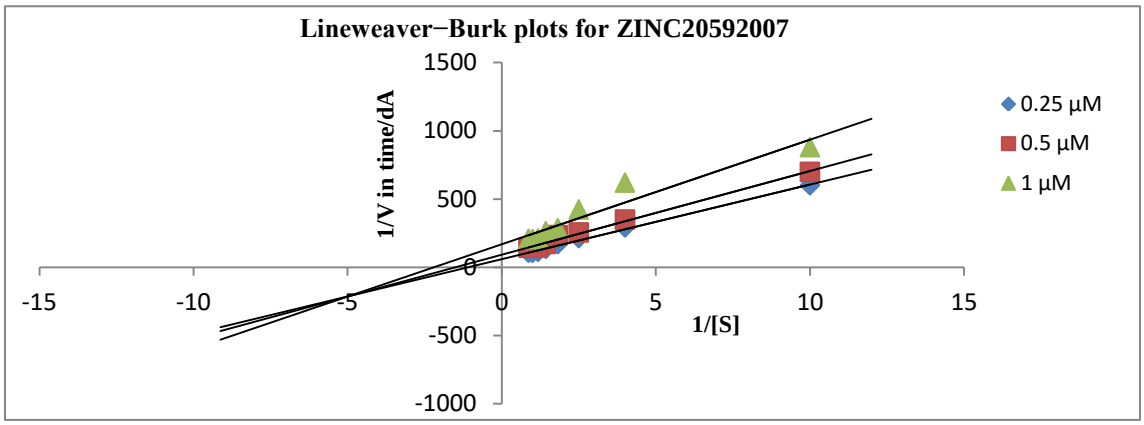

Figure 3.12 Lineweaver-Burk plots from substrate-velocity curves of AChE activity with different substrate concentrations (0.15–1.15 µM) in absence and presence of 0.25, 0.5 and 1 µM of ZINC20592007.

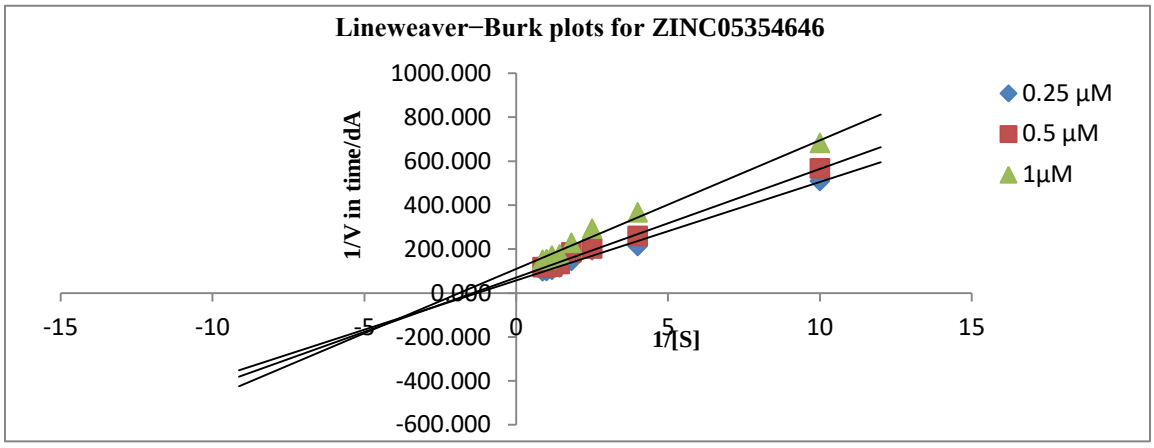

Figure 3.13 Lineweaver-Burk plots from substrate-velocity curves of AChE activity with different substrate concentrations (0.15–1.15 µM) in absence and presence of 0.25, 0.5 and 1 µM of ZINC05354646.

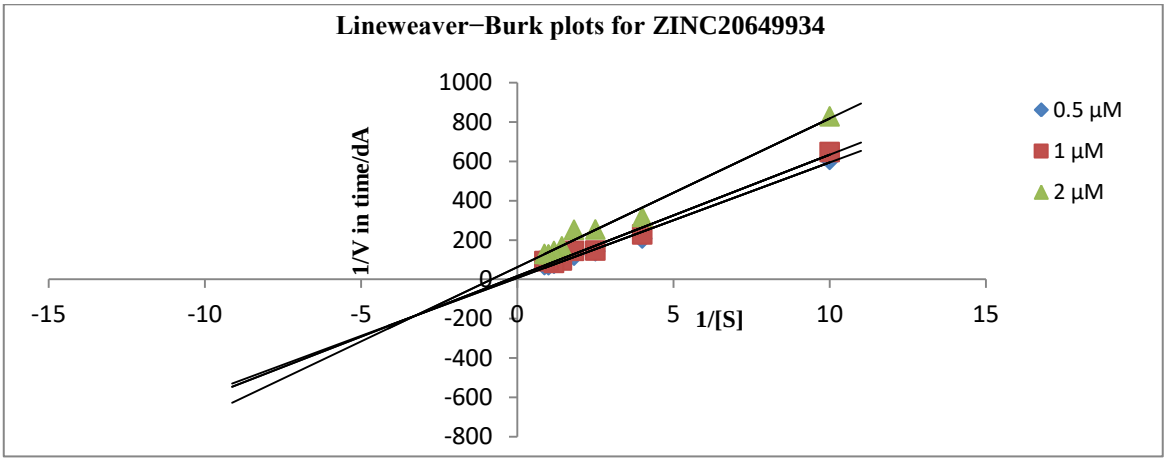

Figure 3.14 Lineweaver-Burk plots from substrate-velocity curves of AChE activity with different substrate concentrations (0.15–1.15 µM) in absence and presence of 0.5, 1 and 2 µM of ZINC20649934.

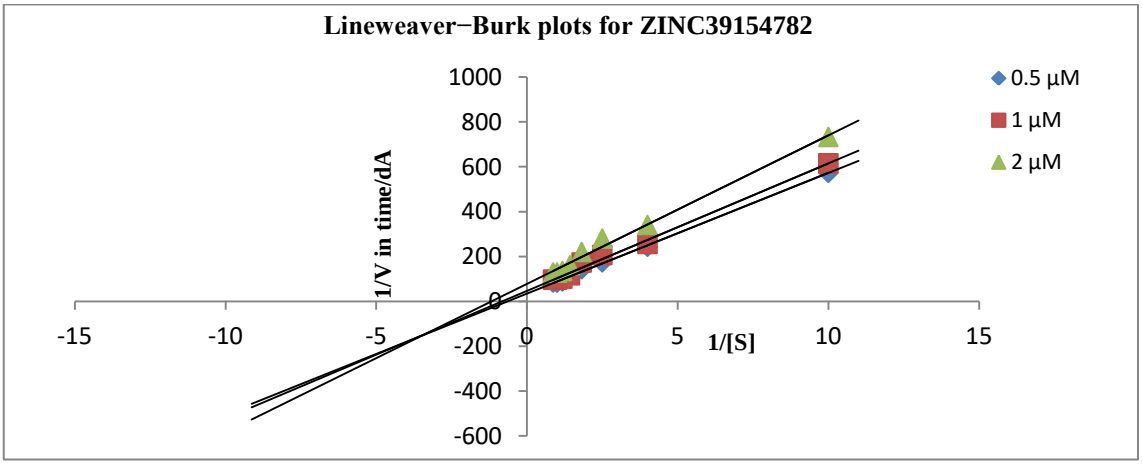

Figure 3.15 Lineweaver-Burk plots from substrate-velocity curves of AChE activity with different substrate concentrations (0.15–1.15µM) in absence and presence of 0.5, 1 and 2 µM of ZINC39154782.

3.3.14 Propidium iodide displacement assay

Particular PAS site binding affinity through Trp286 amino acid residue was established by propidium iodide displacement method. The hits successfully displaced propidium and were proved selective PAS ligands (**Table 3.12**). Molecule ZINC20592007 and ZINC39154782 displaced 100% propidium from PAS of AChE at 3 µM concentration, but ZINC05354646 and ZINC20649934 displaced 57 % and 58% respectively, at the same concentration.

3.3.15 *In vitro* blood-brain barrier permeation assay

The *in vitro* permeability (Pe) of four hits was validated by comparing the experimentally obtained permeability [Pe(exp)] of the nine drugs with reported values of permeation [Pe(ref)] offering a linear relationship,

i.e., Pe(exp) = 1.308 Pe(literature) − 0.8394, (R^2 = 0.9317).

The permeability values (Pe) greater than 4.3×10^{-6} cm s^{-1} were able to penetrate the CNS (calculation details have been illustrated in Chapter 2, Section 2.3.14). The determined permeability values (Pe) of test compounds values (**Table 3.14**) above 4.3×10^{-6} cm s^{-1} were proved that they were comfortable to cross the BBB by passive diffusion.

Table 3.13 The V_{max}, and K_m values of selected hits at various concentrations

Conc. of ZINC 20592009	**0 µM**	**0.25 µM**	**0.5 µM**	**1 µM**
V_{max}	0.003854	0.02164	0.01371	0.01009
K_m	0.976	1.352	0.9819	1.119
Conc. of ZINC95354646	**0 µM**	**0.25 µM**	**0.5 µM**	**1 µM**
V_{max}	0.003854	0.0184	0.01514	0.01218
K_m	0.8966	0.8523	0.7853	0.898
Conc. of ZINC20649934	**0 µM**	**0.5 µM**	**1 µM**	**2 µM**
V_{max}	0.003879	0.03073	0.02251	0.01666
K_m	0.9066	1.31	1.034	1.268
Conc. of ZINC39154782	**0µM**	**0.5 µM**	**1 µM**	**2 µM**
V_{max}	0.003854	0.03091	0.02595	0.01913
K_m	0.8966	1.692	1.577	1.537

3.3.16 Cellular cytotoxicity and neuroprotection assessment

The cellular toxicity and neuroprotectivity of selected hits were evaluated by utilizing human neuroblastoma SH-SY5Y cell line. Cells were exposed to considerably high concentrations of the test compounds (50 µM and 100 µM) for 24h to investigate the

cytotoxicity of compounds. The cell viability was determined by MTT assay. Selected hits showed no toxicity even at high concentrations (**Table 3.15**). The neuroprotective potential was determined by using L-glutamate as excitotoxic agent and ZINC20649934 showed better neuroprotection (**Table 3.15**) than other three. The results are mean ± SEM of at least three independent experiments.

Table 3.14 Permeability determined by BBB-PAMPA study of hits

Compound	Pe [10^{-6} cm s^{-1}][a*]	Prediction[b]
ZINC20592007	5.7±0.20	CNS+
ZINC05354646	9.39±0.36	CNS+
ZINC20649934	5.45±0.79	CNS+
ZINC39154782	5.29±0.31	CNS+

[a]Data expressed as mean ± SEM of three independent experiments. [b]CNS+ indicates good passive CNS permeation; *Permeability (Pe 10^{-6}) express in cm s^{-1}.

Table 3.15 Cell viability, and neuroprotection of hits using SH-SY5Y cell line

Compound	Cell viability (%)[a]		Neuroprotection (%)[b]
	50 µM	100 µM	25 µM
ZINC20592007	98.0±0.34	95.3±0.32	18.2±0.086
ZINC05354646	90.2±0.39	88.7±0.77	20.0±0.061
ZINC20649934	94.8±0.49	93.0±0.45	67.8±0.013
ZINC39154782	98.6±0.55	97.1±0.08	26.3±0.077

[a]Percentage cell viability of SH-SY5Y cells exposed at relatively high concentrations (50 µM and 100 µM) of test compounds. [b]Percentage neuroprotection of SH-SY5Y cells at relatively lower concentrations (25µM) of test compounds against L-glutamate(100 µM).

3.3.17 Molecular dynamics simulation

The analyses of MD simulation of ZINC20592007, ZINC20649934 and donepezil with AChE were performed to establish the binding energy and amino acid residue interactions. RMSD of the protein backbone C-α atoms and individual inhibitor, root mean square fluctuation (RMSF) in the individual amino acid side chain and ligand-AChE interactions were recorded concerning time throughout 50 ns of simulation. The

total energy of dynamic ligand-protein complexes established the stability in last 40ns of complete simulation. Furthermore, temperature, pressure, volume, and potential energy of the complex remained constant, indicating the robustness and reliability of MD simulations. The RMSD of simulation converging between 1.5 and 2.5Å, denoted the stability of macromolecular ligand-protein complexes during 50ns simulation. The RMSF in individual amino acid residues during the entire simulation was below 4.0Å, indicating a lower degree of conformational changes in the side chains.

After initial 10 ns simulation, RMSD of protein backbone C-α along with the ligand RMSD values were stabilized. RMSD plot of RMSD values for protein on the left Y-axis and for ligand these values were displayed on the right Y-axis in **Figure 3.16**; protein backbone in green, and ligand in maroon. The mean RMSD value for donepezil-AChE complex was 2.04Å, whereas ZINC20592007-AChE and ZINC20649934-AChE complexes were 1.76 and 2.11Å respectively. RMSF was useful for characterizing local changes along the protein chain C-α and peaks indicated areas of the protein that fluctuate the most during the simulation. RMSF values of hits and donepezil were below 4.0 Å, indicating less fluctuation and better stability of ligand-protein complex during simulation (**Figure 3.17**). The interaction of hits with AChE, higher than 30% after MD simulation, is provided in **Figure 3.18**.

3.4 Conclusions

A 3D-QSAR and three e-pharmacophore models were developed from known AChE inhibitors, structurally similar to donepezil and available AChE crystal structures with cocrystal ligand at PAS site. Virtual screening of ‘ZINC15’ compounds afforded novel excellent, non-toxic AChE inhibitors. The hits interacted with Trp286, Phe295, Asp74,

Tyr337, and Tyr124 residues of AChE crystal structure through one to three H-bond(s) and one to three pi-pi stacking interaction(s).

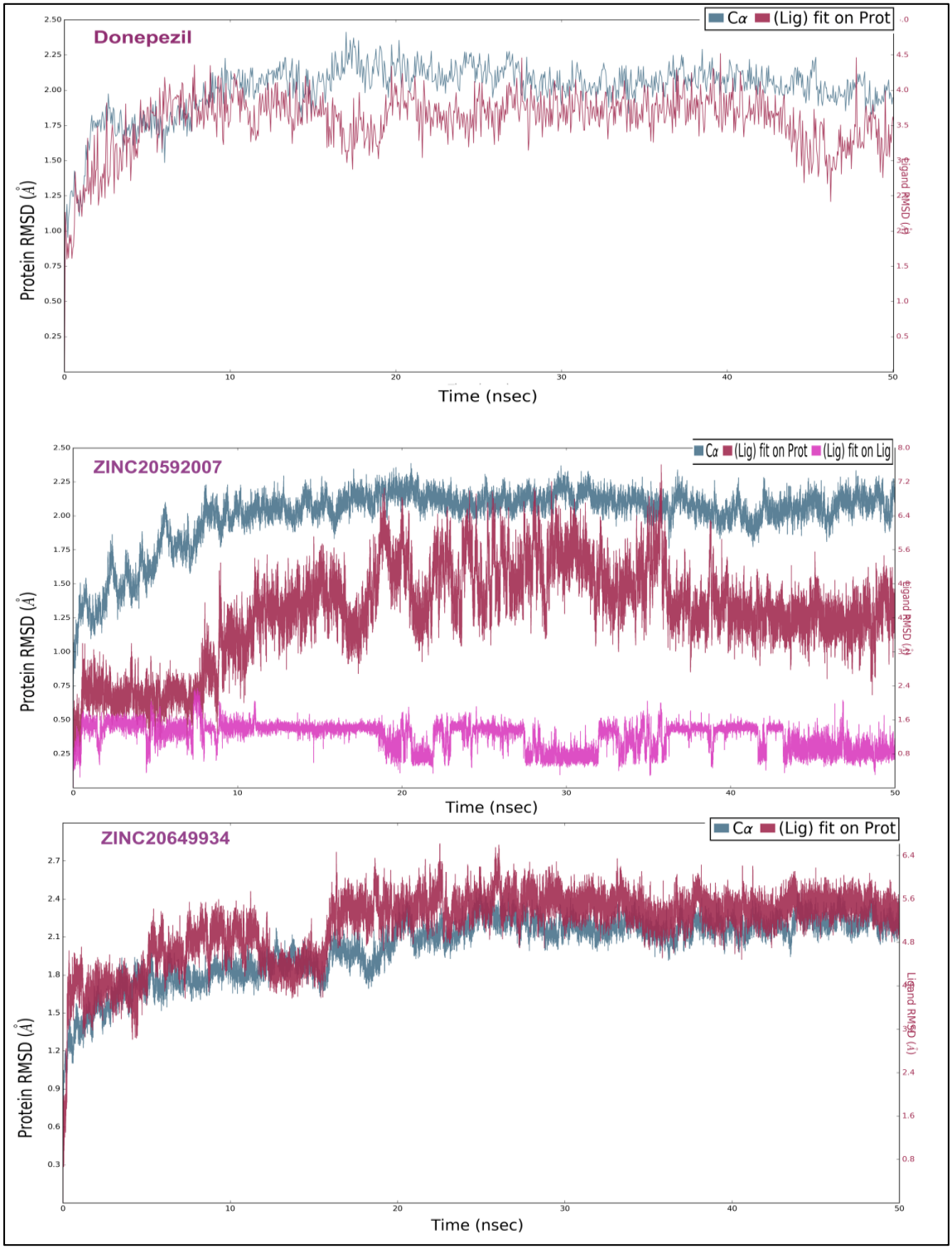

Figure 3.16 RMSD plot of RMSD values (donepezil-AChE, ZINC20592007-AChE, and ZINC20649934-AChE complexes) for protein on the left Y-axis and ligand on the right Y-axis; protein backbone in green, and ligand in maroon.

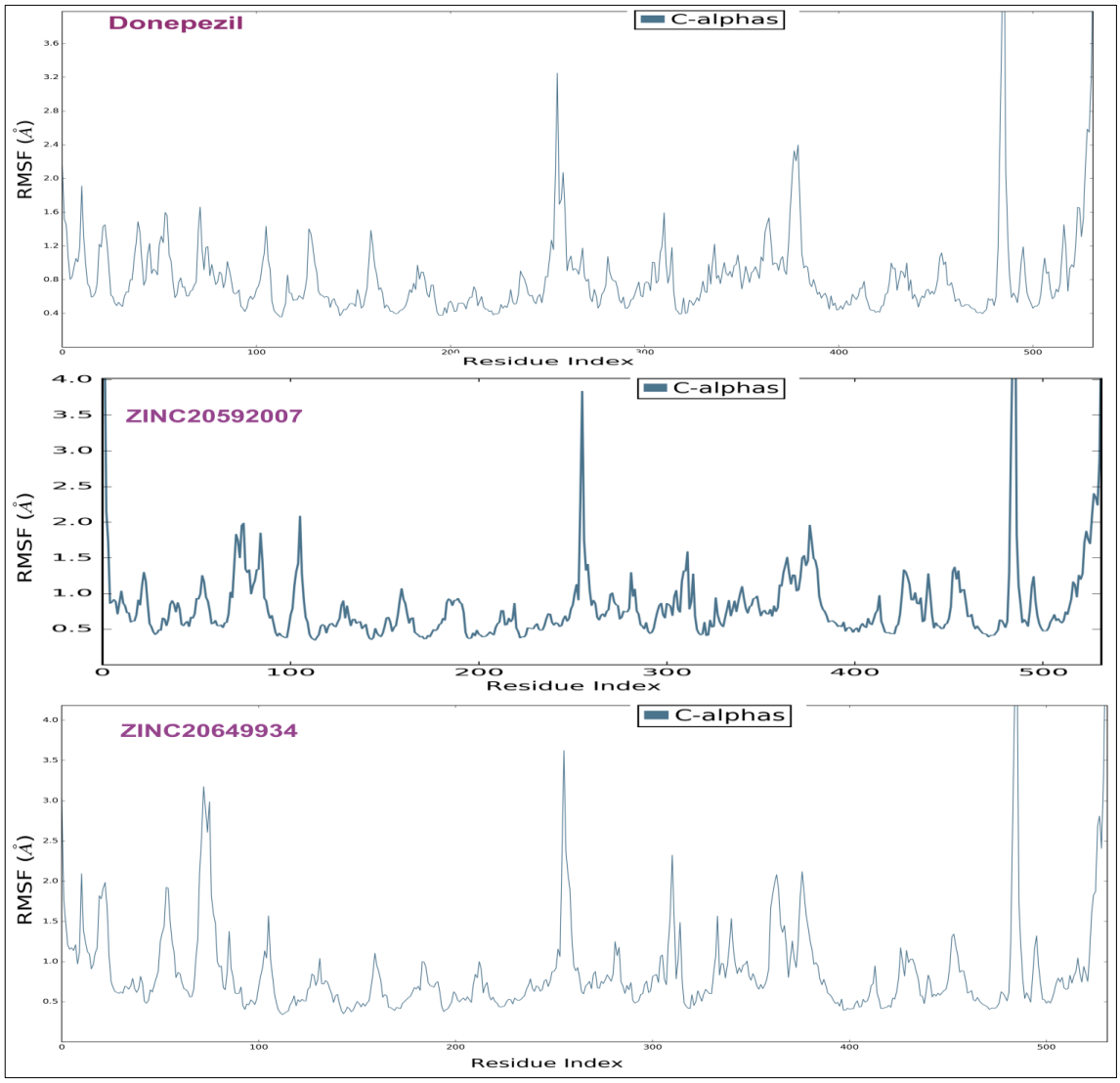

Figure 3.17 RMSF of the protein C-α chain in donepezil-AChE, ZINC20592007-AChE, and ZINC20649934-AChE complexes.

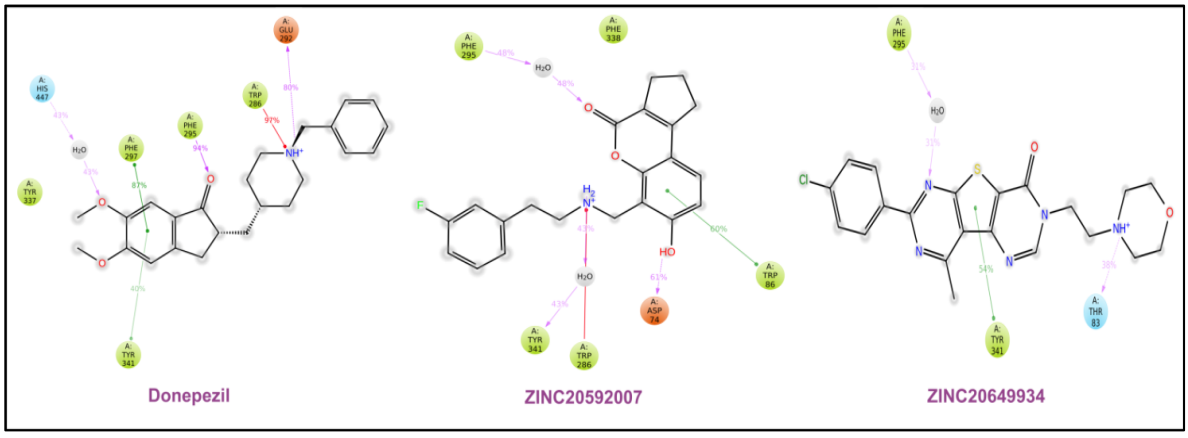

Figure 3.18 Ligand interactions with amino acid residues of AChE after MD.

MD strongly supported that the identified hits bound at PAS of AChE only. *In vitro* enzyme assays, with propidium iodide displacement of ZINC20592007, ZINC05354646, ZINC20649934, and ZINC39154782, also supported the *in silico* results. ZINC20592007 and ZINC39154782, interacting with Try286 amino acid residue, provided 100% propidium displacement at 3μM concentration. The PAS site-selective mimics responded to inhibition of amyloid formation. The hits had attractive Ki values (0.21±0.027, 0.27±0.064, 0.3±0.018, and 0.28±0.032 μM) with insignificant toxicity against neuroblastoma SH-SY5Y cell, good BBB permeability, and neuroprotectivity against L-glutamate induced excitotoxicity. Further, ZINC20592007 molecule had potent, selective AChE inhibition at PAS, *i.e.*, non-competitive, CNS permeability, non-toxicity, neuroprotectivity, and Aβ formation and aggregation inhibition, which increased cholinergic activity and also prevented Aβ aggregation control AD. We consider that these compounds are excellent candidates to develop further as leads for AChE inhibition.

3.5 References

[1] Y. Bourne, P. Taylor, P.E. Bougis, P. Marchot, Crystal structure of mouse acetylcholinesterase a peripheral site-occluding loop in a tetrameric assembly, *Journal of Biological Chemistry*, 274 (1999) 2963–2970.

[2] G. Johnson, S. Moore, The peripheral anionic site of acetylcholinesterase: structure, functions, and potential role in rational drug design, *Current Pharmaceutical Design*, 12 (2006) 217–225.

[3] H. Soreq, S. Seidman, Acetylcholinesterase-new roles for an old actor, *Nature Reviews Neuroscience*, 2 (2001) 294–302.

[4] M. Pakaski, P. Kasa, Role of acetylcholinesterase inhibitors in the metabolism of amyloid precursor protein, *Current Drug Targets-CNS & Neurological Disorders*, 2 (2003) 163–171.

[5] N.P.L. Verhoeff, Acetylcholinergic neurotransmission, and the β-amyloid cascade: implications for Alzheimer's disease, *Expert Review of Neurotherapeutics*, 5 (2005) 277–284.

[6] J. Massoulié, J. Sussman, S. Bon, I. Silman, Structure and functions of acetylcholinesterase and butyrylcholinesterase, *Progress in Brain Research*, 98 (1993) 139–146.

[7] J. Massoulie, S. Bon, The molecular forms of cholinesterase and acetylcholinesterase in vertebrates, *Annual Review of Neuroscience*, 5 (1982) 57–106.

[8] E.O. Campos, A. Alvarez, N.C. Inestrosa, Brain acetylcholinesterase promotes amyloid-β-peptide aggregation but does not hydrolyze amyloid precursor protein peptides, *Neurochemical Research*, 23 (1998) 135–140.

[9] G. Landrum, RDKit: cheminformatics and machine learning software, RDKIT. ORG, (2013).

[10] J. Eichler, A. Anselment, J.L. Sussman, J. Massoulié, I. Silman, Differential effects of" peripheral" site ligands on Torpedo and chicken acetylcholinesterase, *Molecular Pharmacology*, 45 (1994) 335–340.

[11] W.L. Jorgensen, D.S. Maxwell, J. Tirado-Rives, Development and testing of the OPLS all-atom force field on conformational energetics and properties of organic liquids, *Journal of the American Chemical Society*, 118 (1996) 11225–11236.

[12] G.A. Kaminski, R.A. Friesner, J. Tirado-Rives, W.L. Jorgensen, Evaluation and reparametrization of the OPLS-AA force field for proteins via comparison with accurate quantum chemical calculations on peptides, *The Journal of Physical Chemistry B*, 105 (2001) 6474–6487.

[13] L. Di, E.H. Kerns, K. Fan, O.J. McConnell, G.T. Carter, High throughput artificial membrane permeability assay for blood-brain barrier, *European Journal of Medicinal Chemistry*, 38 (2003) 223–232.

[14] D. Lagorce, L. Bouslama, J. Becot, M.A. Miteva, B.O. Villoutreix, FAF-Drugs4: free ADME-tox filtering computations for chemical biology and early stages drug discovery, *Bioinformatics*, 33 (2017) 3658–3660.

[15] W. Porcal, P. Hernández, M. González, A. Ferreira, C. Olea-Azar, H. Cerecetto, A. Castro, Heteroarylnitrones as drugs for neurodegenerative diseases: synthesis, neuroprotective properties, and free radical scavenger properties, *Journal of Medicinal Chemistry*, 51 (2008) 6150–6159.

[16] E. Giacobini, Cholinergic function and Alzheimer's disease, *International Journal of Geriatric Psychiatry*, 18 (2003) S1–S5.

[17] S. Jana, S.K. Singh, Identification of selective MMP-9 inhibitors through multiple e-pharmacophore, ligand-based pharmacophore, molecular docking, and density functional theory approaches, *Journal of Biomolecular Structure & Dynamics*, (2018) 1–22.

[18] J.K. Dhanjal, S. Sharma, A. Grover, A. Das, Use of ligand-based pharmacophore modeling and docking approach to find novel acetylcholinesterase inhibitors for treating Alzheimer's, *Biomedicine & Pharmacotherapy*, 71 (2015) 146–152.

[19] P. Ambure, S. Kar, K. Roy, Pharmacophore mapping-based virtual screening followed by molecular docking studies in search of potential acetylcholinesterase inhibitors as anti-Alzheimer's agents, *BioSystems*, 116 (2014) 10–20.

[20] G. Brahmachari, C. Choo, P. Ambure, K. Roy, *In vitro* evaluation and *in silico* screening of synthetic acetylcholinesterase inhibitors bearing functionalized piperidine pharmacophores, *Bioorganic & Medicinal Chemistry*, 23 (2015) 4567–4575.

[21] Y. Zhang, S. Zhang, G. Xu, H. Yan, Y. Pu, Z. Zuo, The discovery of new acetylcholinesterase inhibitors derived from pharmacophore modeling, virtual screening, docking simulation and bioassays, *Molecular BioSystems*, 12 (2016) 3734–3742.

[22] S. Bag, R. Tulsan, A. Sood, S. Datta, M. Torok, Pharmacophore modeling, virtual and *in vitro* screening for acetylcholinesterase inhibitors and their effects on Amyloid-β self-assembly, *Current Computer-Aided Drug Design*, 9 (2013) 2–14.

[23] R. Malik, B.S. Choudhary, S. Srivastava, P. Mehta, M. Sharma, Identification of novel acetylcholinesterase inhibitors through e-pharmacophore-based virtual screening and molecular dynamics simulations, *Journal of Biomolecular Structure & Dynamics*, (2016) 1–17.

[24] M. Shidore, J. Machhi, K. Shingala, P. Murumkar, M.K. Sharma, N. Agrawal, A. Tripathi, Z. Parikh, P. Pillai, M.R. Yadav, Benzylpiperidine-linked diarylthiazoles as potential anti-Alzheimer's agents: synthesis and biological evaluation, *Journal of Medicinal Chemistry*, 59 (2016) 5823–5846.

[25] S. Release, 1: Maestro, version 10.1, Schrödinger, LLC, New York, NY, (2015).

[26] S.L. Dixon, A.M. Smondyrev, S.N. Rao, PHASE: a novel approach to pharmacophore modeling and 3D database searching, *Chemical Biology & Drug Design*, 67 (2006) 370–372.

[27] P. Pratim Roy, S. Paul, I. Mitra, K. Roy, On two novel parameters for validation of predictive QSAR models, *Molecules*, 14 (2009) 1660–1701.

[28] K. Loving, N.K. Salam, W. Sherman, Energetic analysis of fragment docking and application to structure-based pharmacophore hypothesis generation, *Journal of Computer-Aided Molecular Design*, 23 (2009) 541–554.

[29] N.K. Salam, R. Nuti, W. Sherman, Novel method for generating structure-based pharmacophores using energetic analysis, *Journal of Chemical Information and Modeling*, 49 (2009) 2356–2368.

[30] T.A. Halgren, R.B. Murphy, R.A. Friesner, H.S. Beard, L.L. Frye, W.T. Pollard, J.L. Banks, Glide: a new approach for rapid, accurate docking and scoring. 2. Enrichment factors in database screening, *Journal of Medicinal Chemistry*, 47 (2004) 1750–1759.

[31] J.J. Irwin, T. Sterling, M.M. Mysinger, E.S. Bolstad, R.G. Coleman, ZINC: a free tool to discover chemistry for biology, *Journal of Chemical Information and Modeling*, 52 (2012) 1757–1768.

[32] S.L. Dixon, A.M. Smondyrev, E.H. Knoll, S.N. Rao, D.E. Shaw, R.A. Friesner, PHASE: a new engine for pharmacophore perception, 3D QSAR model development, and 3D database screening: 1. Methodology and preliminary results, *Journal of Computer-Aided Molecular Design*, 20 (2006) 647–671.

[33] G.L. Ellman, K.D. Courtney, V. Andres Jr, R.M. Featherstone, A new and rapid colorimetric determination of acetylcholinesterase activity, *Biochemical Pharmacology*, 7 (1961) 88–95.

[34] H. Motulsky, Prism 5 statistics guide, 2007, *GraphPad Software*, 31 (2007) 39–42.

[35] R.A. Friesner, R.B. Murphy, M.P. Repasky, L.L. Frye, J.R. Greenwood, T.A. Halgren, P.C. Sanschagrin, D.T. Mainz, Extra precision glide: Docking and scoring incorporating a model of hydrophobic enclosure for protein-ligand complexes, *Journal of Medicinal Chemistry*, 49 (2006) 6177–6196.

[36] H. Wang, R. Aslanian, V.S. Madison, Induced-fit docking of mometasone furoate and further evidence for glucocorticoid receptor 17α pocket flexibility, *Journal of Molecular Graphics and Modelling*, 27 (2008) 512–521.

[37] R.A. Friesner, J.L. Banks, R.B. Murphy, T.A. Halgren, J.J. Klicic, D.T. Mainz, M.P. Repasky, E.H. Knoll, M. Shelley, J.K. Perry, Glide: a new approach for rapid, accurate docking and scoring. 1. Method and assessment of docking accuracy, *Journal of Medicinal Chemistry*, 47 (2004) 1739–1749.

[38] N. Huang, C. Kalyanaraman, J.J. Irwin, M.P. Jacobson, Physics-based scoring of protein-ligand complexes: enrichment of known inhibitors in large-scale virtual screening, *Journal of Chemical Information and Modeling*, 46 (2006) 243–253.

[39] M. Jin, N. Shepardson, T. Yang, G. Chen, D. Walsh, D.J. Selkoe, Soluble amyloid β-protein dimers isolated from Alzheimer cortex directly induce Tau hyperphosphorylation and neuritic degeneration, *Proceedings of the National Academy of Sciences*, 108 (2011) 5819–5824.

[40] Z. Yu, M.P. Jacobson, R.A. Friesner, What role do surfaces play in GB models? A new-generation of surface-generalized born model based on a novel gaussian surface for biomolecules, *Journal of Computational Chemistry*, 27 (2006) 72–89.

[41] P.D. Lyne, M.L. Lamb, J.C. Saeh, Accurate prediction of the relative potencies of members of a series of kinase inhibitors using molecular docking and MM-GBSA scoring, *Journal of Medicinal Chemistry*, 49 (2006) 4805–4808.

[42] G.M. Morris, D.S. Goodsell, R.S. Halliday, R. Huey, W.E. Hart, R.K. Belew, A.J. Olson, Automated docking using a Lamarckian genetic algorithm and an empirical binding free energy function, *Journal of Computational Chemistry*, 19 (1998) 1639–1662.

[43] E.M. Duffy, W.L. Jorgensen, Prediction of properties from simulations: free energies of solvation in hexadecane, octanol, and water, *Journal of the American Chemical Society*, 122 (2000) 2878–2888.

[44] C.A. Lipinski, F. Lombardo, B.W. Dominy, P.J. Feeney, Experimental and computational approaches to estimate solubility and permeability in drug discovery and development settings, *Advanced Drug Delivery Reviews*, 23 (1997) 3–25.

[45] F. Ntie-Kang, An *in silico* evaluation of the ADMET profile of the StreptomeDB database, *SpringerPlus*, 2 (2013) 353.

[46] J. Matysiak, Evaluation of electronic, lipophilic and membrane affinity effects on antiproliferative activity of 5-substituted-2-(2,4-dihydroxyphenyl)-1, 3, 4-thiadiazoles against various human cancer cells, *European Journal of Medicinal Chemistry*, 42 (2007) 940–947.

[47] P.M. Gill, B.G. Johnson, J.A. Pople, M.J. Frisch, The performance of the Becke-Lee-Yang-Parr (B-LYP) density functional theory with various basis sets, *Chemical Physics Letters*, 197 (1992) 499–505.

[48] P. Stephens, F. Devlin, C. Chabalowski, M.J. Frisch, *Ab initio* calculation of vibrational absorption and circular dichroism spectra using density functional force fields, *The Journal of Physical Chemistry*, 98 (1994) 11623–11627.

[49] Y. Zheng, M. Zheng, X. Ling, Y. Liu, Y. Xue, L. An, N. Gu, M. Jin, Design, synthesis, quantum chemical studies and biological activity evaluation of pyrazole–benzimidazole derivatives as potent Aurora A/B kinase inhibitors, *Bioorganic & Medicinal Chemistry Letters*, 23 (2013) 3523–3530.

[50] P. Masson, W. Xie, M.-T. Froment, V. Levitsky, P.-L. Fortier, C. Albaret, O. Lockridge, Interaction between the peripheral site residues of human butyrylcholinesterase, D70 and Y332, in binding and hydrolysis of substrates, Biochimica et Biophysica Acta (BBA)-Protein *Structure and Molecular Enzymology*, 1433 (1999) 281–293.

[51] P.R. Twentyman, M. Luscombe, A study of some variables in a tetrazolium dye (MTT) based assay for cell growth and chemosensitivity, *British Journal of Cancer*, 56 (1987) 279–285.

[52] B. Sameem, M. Saeedi, M. Mahdavi, H. Nadri, F.H. Moghadam, N. Edraki, M.I. Khan, M. Amini, Synthesis, docking study and neuroprotective effects of some

novel pyrano [3, 2-c] chromene derivatives bearing morpholine/phenylpiperazine moiety, *Bioorganic & Medicinal Chemistry*, 25 (2017) 3980–3988.

[53] M.R. Berthold, N. Cebron, F. Dill, T. Gabriel, T. Kötter, T. Meinl, P. Ohl, C. Sieb, K. Thiel, B. Wiswedel, KNIME: The Konstanz Information Miner Studies in Classification, Data Analysis, and Knowledge Organisation (GfKL 2007) *Springer*, (2007).

[54] X. Di, J. Yan, Y. Zhao, J. Zhang, Z. Shi, Y. Chang, B. Zhao, L-theanine protects the APP (Swedish mutation) transgenic SH-SY5Y cell against glutamate-induced excitotoxicity via inhibition of the NMDA receptor pathway, *Neuroscience*, 168 (2010) 778–786.